Source Processes and Dynamic Rupture Models of Three Inland Earthquakes in the Northwestern Chubu District, Central Honshu Japan(Dissertation_全文)

AUTHOR(S):

Mikami, Naoya

(2)

主論文 1

Source Processes and Dynamic Rupture Models of Three Inland Earthquakes in the Northwestern Chubu District, Central Honshu, Japan

Naoya MIKAMI

Seismological Observatory, Japan Meteorological Agency,
Matsushiro, Nagano 381-12, Japan

submitted to Geophys. J. Int.

January, 1992

Abstract

The rupture processes of three inland earthquakes in the northwestern Chubu district, the 1984 NaganoKen-Seibu earthquake, the 1969 GifuKen-Chubu earthquake, and the 1961 Kita-Mino earthquake, have been investigated by the inversion of JMA strong motion seismograms. We have successfully obtained the slip distribution and the rupture propagation on the fault that satisfy the strong motion data for each of the three earthquakes. The dynamic rupture models reconstructed from these kinematic models have been discussed. The dynamic models reveal that both the stress drop and the strength excess are heterogeneously distributed over the fault for all the three earthquakes. There exist zones of high stress drop and high strength excess at the shallow part of the fault. The rupture processes are more complicated when compared with those of two earthquakes in the Izu region. These features suggest that the properties of the shallow crust in the Chubu region may be more heterogeneous with higher frictional strength than those in the Izu region.

1. Introduction

As a quantitative model of earthquake faulting, Haskell (1969) model has been widely used for long years. In this model, fault displacement propagates along the length of a rectangular fault with a constant rupture velocity. The displacement is assumed to be constant over the fault and the time function is assumed to be of a ramp function with a constant rise time. This simple model has been applied to many large earthquakes and successfully explained the general feature of earthquake faulting (e.g. Kanamori, 1972). Actual waveforms of large earthquakes are, however, more complicated than those expected from the Haskell model. Recently, to interpret complex waveforms and to infer detailed faulting processes, waveform inversion techniques have been developed. For many large earthquakes, kinematic parameters, that is slip distribution and rupture propagation on a fault, have been recovered by an inversion of near-field strong motion records, teleseismic body waves, and surface waves (e.g. Hartzell and Heaton, 1983; Mori and Shimazaki, 1985; Kikuchi and Fukao, 1985; Fukuyama and Irikura, 1986; Takeo and Mikami, 1987). Among these waveform data, near-field records are most crucial to recover the detailed source processes of these earthquakes. The 1979 Imperial Valley earthquake provided a number of valuable strong motion records observed within an epicentral distance of several tens of kilometers. Using this data set, several studies revealed the detailed rupture history of this earthquake (e.g. Olson and Aspel, 1982; Hartzell and Heaton, 1983; Archuleta, 1984). In Japan, since 1960's strong motion seismograph network

of Japan Meteorological Agency (JMA) has been operated, and several strong motion records within an epicentral distance of about 100 km have been obtained for inland or near-coast earthquakes of moderate magnitudes.

Kinematic fault models obtained by these waveform inversions show heterogeneous distribution of slip and irregular rupture propagation on the fault. These inhomogeneities are interpreted by two models, that is "barrier" (Aki, 1979) and "asperity" (Kanamori, 1981) models. The barrier indicates a strong part of the fault which arrested the rupture. On the other hand, the asperity is a strong part which causes large stress drop. It now becomes very important for comprehensive understanding of detailed source process of large earthquakes to connect kinematic rupture models with dynamic ones.

An attempt has been made to estimate dynamic parameters from the waveform inversion based on dynamic rupture models (Fukuyama and Mikumo, 1991). However, it is difficult to estimate dynamic source parameters stably. Another approach to connect kinematic and dynamic models is a reproduction of kinematic rupture models by using dynamic crack models. Mikumo et al. (1987) simulated the source process of the 1984 NaganoKen-Seibu earthquake with a three-dimensional spontaneous dynamic shear crack model. Synthesizing a large number of dynamic models, Quin (1990) reproduced kinematic parameters of the 1979 Imperial Valley earthquake. Recently, Miyatake (1991) developed a simple method which converts the kinematic rupture parameters on a fault into dynamic parameters for a strike-slip vertical fault. For thrust

faults, Mikumo et al. (1991) recovered dynamic rupture process from kinematic parameters.

In this paper, kinematic models of detailed rupture processes of three inland earthquakes, the 1984 NaganoKen-Seibu earthquake, the 1969 GifuKen-Chubu earthquake, and the 1961 Kita-Mino earthquake, that occurred in the northwestern Chubu district in central Honshu, Japan, are investigated by the inversion of near-field strong motion waveform records. These kinematic models are converted into dynamic models by the methods of Miyatake (1991) and Mikumo and Miyatake (1991). The kinematic and dynamic rupture models are compared with aftershock distributions. On the basis of the results, the distribution of asperities and barriers on the fault is discussed in detail.

In Fig. 1, the epicenters of the earthquakes analyzed in this study are shown together with the distribution of Quaternary active faults and active volcanoes. The northwestern part of the Chubu district is a mountainous region which is bounded on the east by the Hida mountain range and on the west by the Ryohaku mountains. There exist many conjugate sets of Quaternary faults, and this region is recognized as one of the most active Quaternary tectonic regions in Japan. Active volcanoes also exist in both the Hida mountain range and the Ryohaku mountains. A possible relation between earthquake source processes and the tectonic features in this region is also discussed in this paper.

2. Method of Analysis

The rupture processes of three earthquakes are investigated by applying the waveform inversion method by Takeo (1987). This method is briefly outlined as follows.

An entire fault plane is divided into a number of subfaults which start rupturing with arbitrary magnitudes at arbitrary times. To reduce the number of unknown parameters, the orientation of and the rupture duration at each subfault are given beforehand. The i-th component of the synthetic seismogram at any time t at a particular station is given by the summation of weighted Green's functions,

$$u_i(t;m_j,t_j^s)=\sum_j m_j w_{ij}(t;t_j^s),$$

where m_j and t_j^s denote the seismic moment and the starting time of rupture at the j-th subfault, respectively. w_{ij} is the Green's function which represents the i-th component of the seismogram excited by the rupture on the j-th subfault. For each subfault, w_{ij}'s are first calculated for a point source at the center of the subfault and then convolved with a parabolic ramp function corresponding to the rupture duration for the subfault. Directivity associated with rupture propagation on the entire fault plane is automatically included in the synthetic seismogram because u_i is calculated by the summation of the Green's functions which are subject to the time shifts, t_j^s.

The observed strong motion seismograms are digitized at a time step of t; then, the i-th component of the observations ($O_i(t)$) is expressed as a discrete time series $O_i(t_k)$, k=1 N_i, where N_i is the total number of the discretized points for the i-th

component. The synthetic seismogram is calculated at the same time interval and is expressed as $u_i(t_k)$. Then, m_j and t_j^s are determined by minimizing the sum of a square error $S(m_j, t_j^s)$, defined by

$$S(m_j, t_j^s) = \sum_{j,k} [O_i(t_k) - u_i(t_k; m_j, t_j^s)]^2.$$

To solve this problem, we employ the Householder technique and the modified Marquardt technique for linear and nonlinear inversion algorisms, respectively. The inversion is performed iteratively from the starting model.

Our model assumes that each subfault has a fixed slip orientation, a fixed fault plane geometry, and a fixed rupture duration. If these assumed values are not suitable for actual earthquake, it is expected that the residual value S becomes large or the solution appears unrealistic and physically unreasonable. In such cases, we have to modify the assumed parameters. The fault geometry and slip orientation are determined by aftershock distribution and focal mechanism solution from P-wave first motions. These are not changed in our analyses. The rupture durations at subfaults are assumed from its size and are changed slightly to select an optimum value.

Because of nonlinearity of the problem, the solutions of this inversion method depend on the starting model parameters. It is our procedure that a number of starting models are tested and then the best solution is chosen by the following criteria. Firstly, any solutions with large negative moment or unreasonably irregular rupture propagation are abandoned. If there are several solutions which show equally small residuals, the solution having

the smoothest rupture process is taken as the best one. This is because it is a fundamental assumption in our analysis that the rupture process does not unreasonably fluctuate over a fault plane.

Green's functions for horizontally layered media are calculated by the discrete wave number/finite-element method (Alekseev and Mikhailenko, 1980; Olson, 1982) or by the use of reflection-transmission matrices (e.g. Kennet and Kerry, 1979) and the discrete wavenumber method (Bouchon, 1980), assuming an anelastic structure (e.g. Takeo, 1985). The Green's functions obtained by these methods include all types of body and surface waves and near-field terms. Crustal structure models to calculate Green's functions also affect the inversion solutions. Three crustal models appropriate to the region of interest shown in Fig. 2 are used in this study.

The seismograms recorded by Japan Meteorological Agency (JMA) mechanical strong motion seismographs were used in the present analysis. The natural period of seismographs is 6 sec for the horizontal components, and 5 sec for the vertical components, respectively. The damping constant is about 0.5 and the magnification is 1. Correcting the distortion due to the mechanism of the recording system, we digitized the records at a sampling rate of 4 Hz. The digital Chevyshev low-pass filter was applied to the data before the inversion analysis to cut frequency components higher than 1.0 Hz.

3. Results

1) The 1984 NaganoKen-Seibu earthquake

The NaganoKen-Seibu earthquake with a magnitude of 6.8 occurred in the western part of Nagano prefecture on September 14, 1984. The station distribution used in this study is shown in Fig. 3 with the epicenter of the main shock. This event was a multiple shock and a small foreshock preceded the main shock by about 1.5 sec (Japan Meteorological Agency, 1986). Focal mechanism solutions for both a foreshock and the main shock were determined by using P-wave first motion data from JMA and WWSSN records (Fig. 4). Both events show strike-slip faulting with an NW-SE maximum pressure axis. These fault plane solutions are consistent with those of other earthquakes that occurred in this region (e.g. Ichikawa, 1971). As the foreshock was not clearly recognized in strong motion records, the solution for the main shock was used as the mechanism for each subfault. The nodal plane of the main shock, striking in the direction N70°E, agrees well with the strike of aftershock distribution. Therefore, we consider this nodal plane to be the fault plane. The dip of the fault plane is 72°. The extent of the fault plane of the main shock is assumed to be 12km long and 9km wide from the spatial distribution of aftershocks which occurred within 3 hours after the main event. The depth to the top of the fault is assumed to be 1km. The fault plane is divided into twelve 3km x 3km subfaults. In Fig. 5, the aftershocks which occurred before the largest aftershock and the locations of the divided subfaults are shown. The hypocenter of the main shock and the largest after-

shock are also plotted.

Records of the horizontal components of JMA strong motion seismographs at Iida (IID), Takayama (TKY), Matsumoto (MTM), Gifu (GIF) and Matsushiro (MAT) are used for the inversion analysis. As shown in Fig. 3, these stations are distributed around the main shock epicenter, and their epicentral distances are 43, 46, 60, 86, and 99 km respectively. The rupture duration at each subfault is assumed to be 1.5 sec.

Two different crustal models (Structure A and B in Fig. 2) were assumed for the calculation of Green's functions. For these two crustal models, rupture processes were estimated independently. We investigated several cases of rupture propagation, which include the rupture nucleating at subfaults surrounding the given main shock hypocenter and at the deepest ones, as the initial models. For cases in which the rupture nucleated at the middle or deepest depth subfaults, the obtained solutions were found to be physically unreasonable. Although these solutions showed equally small residuals with the other solutions, a large negative seismic moment was obtained on the middle part of the fault and the rupturing times showed a chaotic disorder. We finally adopted the models in which the rupture started from the shallowest subfaults.

The dislocation distribution and rupture propagation inferred from the final solutions for the two different crustal models are shown in Fig. 6. Because the moments obtained for the deepest subfaults except at the east end were very small and unstable, the moments for these subfaults were fixed to be zero in the case

of Structure A. In spite of some difference in the velocity structures used in the calculation, it is found that the overall characteristics of the final models are similar to each other.

These models indicated that the rupture initiated at a shallow point near the center of the fault, spread circularly over the entire fault surface within about 3 sec. The dislocation in the deeper part of the fault was small and the moment release took place mainly at shallow depths in the eastern and western sections. The synthetic seismograms calculated from these final models are compared with the observed seismograms in Fig. 7. As shown in the figure, the waveforms and amplitudes on the observed and synthetic seismograms agree well.

In Fig. 8, the slip distribution is compared with the distribution of aftershocks. There are few aftershocks at the center and the shallow part of the fault. Most of large aftershocks are located in the deeper part of the fault where small slip took place. The total seismic moments for models A and B are 2×10^{25} dyne-cm and 4×10^{25} dyne-cm respectively.

Yamashina and Tada (1986) inferred the fault parameters of this earthquake based on the changes of the distances between triangulation points. Their results indicate that the average dislocation of about 1.6 m occurred on the fault plane with a 14km length and a 2 km width. The upper margin of their fault is located about 0.5 km deep. Their model is generally consistent with our models.

Yoshida and Koketsu (1990) also analyzed this earthquakes using the same strong motion data combined with geodetic data. Although

the shallow large slip and rupture propagation pattern in their results are similar to those in our models, the zone of large slippage is not separated into two parts in their analysis. This difference may be caused by some difference in the inversion method, especially in the smoothing constraints of theirs.

2) The 1969 GifuKen-Chubu earthquake

The GifuKen-Chubu earthquake with a magnitude 6.6 occurred in the central part of Gifu Prefecture on September 9, 1969. The hypocenter distribution of aftershocks of this earthquake has been investigated in detail by Watanabe and Kuroiso (1970). Hamada (1987) also studied the aftershock distribution by hypocenter relocation using JMA data. Based on these results, we assumed the fault plane with dimensions of a 20 km length and a 11.2 km width. The fault plane was divided here into twenty 4km (length) x 2.8km (width) subfaults. Mikumo (1973) analyzed seismic and geodetic data of this earthquake and found that the event was caused by left-lateral strike-slip motion along a vertical fault plane with a strike of N27°W. This mechanism (Fig. 9) is adopted for each subfault. Figure 10 shows the division of subfaults with the aftershock distribution obtained by Hamada (1987).

Horizontal components of the seismograms recorded at eight stations, Gifu (GIF), Takayama (TKY), Iida (IID), Nagoya (NAG), Fukui (FUK), Tsuruga (TSR), Kanazawa (KAN), and Matsumoto (MTM) shown in Fig. 11 were used for the inversion analysis. The epicentral distances to these stations are shorter than 100 km.

Azimuthal coverage of the stations and the data quality for this event are the best among the three earthquakes analyzed in this paper. For these reasons, several tests of inversion analysis were performed.

The results for several models with different data sets, different crust models or different starting models are summarized in Fig. 12. These results are the best one under each of these conditions.

In order to see the stability of the solutions, we divided the whole data set into 2 different sets and applied the inversion to the different data. The solutions using the three stations (GIF, TKY, IID) at nearest distances and the four stations (NAG, TSR, KAN, MTM) at medium distances are called models a and b in Fig. 12, respectively. Although the data are independent, the distribution of the obtained moment release on the fault for the both models is found to be very similar to each other. This indicates high reliability of the solutions for the moment distribution.

The results from all eight stations for two different velocity structures (Structure C and A) are also shown as models c and d in Fig. 12. The patterns of the moment release for models a to d are very similar, but the rupture propagation patterns are slightly different. These results show that the rupture started at the shallowest depth at the center of the fault. The rupture velocities are faster for models with velocity structure C. The total moments obtained are smaller for models using all station data. The residuals for model c is about 1.6 times as large as

that for model d.

A reasonable solution can also be obtained (model e in Fig. 12) for the rupture nucleated at the deepest subfault. Although the rupture propagation pattern in this case is quite different from that for the above four models, the moment distribution resembles to other models. In this case, the residual value is 1.3 times as large as that of model d. Therefore, we adopted model d as the final model. The focal depth of the main shock redetermined by Hamada (1987) is shallow, supporting the final model in which the rupture initiated at a shallow depth. Fig. 13 shows a comparison between the observed seismograms and the corresponding synthetic seismograms calculated by the final model. It is found that a fit of the synthetics to the observations is excellent.

The final model is shown in Fig. 14 with the hypocenter distribution of aftershocks determined by Hamada (1987). The final model indicates that the rupture initiated at the central shallow section of the fault and spread firstly downward and then towards bilaterally both directions with a slightly incoherent pattern. The largest slip of 1.7m occurred at the northwest of and just below the hypocenter and this subfault appears to have delayed the rupture propagation. It may be inferred that this large-slip zone has a high frictional strength which is higher than the initial shear stress enough to act as a barrier at the initial stage of the rupture process. After the rupture propagates to the surrounding zones, the shear stress in the zone might exceed the frictional strength, and then the zone was broken with a high stress drop. The displacement at the shallow

part and the southeastern half of the fault was quite small. It is to be noted that most of the aftershocks are distributed at the shallow part of the fault where small dislocations occurred, and that several aftershocks appear to have occurred around the part of the largest slip. The average slip over the entire fault was 0.68m, and total seismic moment was 5.4×10^{25} dyne-cm.

Mikumo (1973) analyzed this earthquakes using seismic and geodetic data, and found that slips over the northwestern part of the fault might be considerably larger than the average slip of 0.6-0.7 m. Our final model is very consistent with the Mikumo's results.

3) The 1961 Kita-Mino earthquake

The Kita-Mino earthquake with a magnitude of 7.0 occurred in the border region of Gifu, Fukui, and Ishikawa Prefectures on August 19, 1961. Kawasaki (1975) analysed the source process of this earthquake based on seismological and geodetic data and found that this event is a result of right-lateral reverse faulting on a fault plane with a length of 12 km and a width of 10 km. The fault plane solution determined by Kawasaki (1975) is shown in Fig. 15. The aftershock distribution of this earthquake relocated by Hamada (1987) extends for about 20 km southwest from the main shock epicenter. Based on these results, we assumed a fault plane with a strike of N20°E and dip of 60° whose length and width were 16 km and 12 km, respectively. The fault was divided here into twelve 4 km x 4 km subfaults. In Fig. 16, the subfault arrangement with the aftershock distribution by Hamada

(1987) is shown.

The station distribution and the epicenter of the main shock are shown in Fig. 17. The horizontal and vertical components of the seismograms recorded at Fukui (FUK), Takayama (TKY), Tsuruga (TSR), Gifu (GIF), Toyama (TOY), and Hikone (HIK) were used for the inversion analysis, but the seismograms recorded at the stations indicated by open circle in Fig. 17 were not used because of their poor quality. The velocity model of Structure A (Fig. 2) was used to calculate Green's functions. A source duration at each subfault was assumed to be 3 sec.

Several solutions with equally small residuals were obtained by the inversion. These solutions are shown in Fig. 18. We could not select the best model only by the residual values. These three solutions are different in the rupture progress and slip distribution patterns, especially in the southwestern half of the fault. We select the final model based on the smoothness of rupturing. Since model a provides the smoothest rupture propagation pattern and slip distribution, this was adopted as the final model. The synthetic seismograms calculated from the final model are compared with the observed seismograms in Fig. 19. It is to be noted that the synthetic and observed seismograms agree very well.

The final model is shown in Fig. 20 together with aftershock distribution obtained by Hamada (1987). The model shows that the rupture started at the northeastern end of the fault and propagated rather smoothly, decelerating in the southwestern part of the fault. The slip in the northeastern half of the fault

was large especially at the shallow section. The rupture process at the southwestern half of the fault is ambiguous, because the three solutions with equally small residuals show different features. However, the deceleration of rupture propagation and the relatively small slip at the southwestern part of the fault are common features in all these models (see Fig. 18). After-shocks are concentrated at the southwestern shallow part of the fault where small slip occurred. The average slip on the entire fault and total seismic moment are 0.9 m and 5×10^{25} dyne-cm, respectively.

Kawasaki (1975) determined the seismic moment to be 9×10^{25} dine-cm based mainly on leveling measurement. Our solutions estimated from strong motion records are somewhat smaller than the Kawasaki's result. We calculated theoretical static displacements for the final model by using the program of Sato and Matsu'ura (1974). Assuming that the effect of the Fukui earthquake is smaller than that estimated by Kawasaki, our results fit well the observed spatial variations of the vertical displacements. However, the calculated displacement amplitudes are smaller than the observed values. Since the leveling route passed near the southwestern end of the fault where many shallow aftershocks occurred, the discrepancy might be caused by these aftershocks.

4. Discussion

The reliability of the obtained solutions is one of the most important problems in the waveform inversion analysis to discuss the rupture processes of earthquake faulting. Actually, relatively large inconsistencies were detected among several kinematic models of the 1979 Imperial Valley earthquake obtained by waveform inversions (e.g. Olson and Aspel, 1982; Hartzell and Heaton, 1983; Archuleta, 1984). In the case of the 1984 NaganoKen-Seibu earthquake, the results of our analysis and of Yoshida and Koketsu (1990) show somewhat different features of slip distribution. Also, Iida et al. (1990) pointed out that station distribution used for the inversion analysis largely affected the solutions. However, it is difficult to confirm the accuracy of inversion results directly.

The inversion analysis using independent data set of the GifuKen-Chubu earthquake shows that the slip distribution has been stably obtained and that the data even from 3 or 4 stations could resolve the slip distribution. The total seismic moment and the rupture propagation pattern obtained here are, however, somewhat different depending on the data set selected. Since the azimuthal coverage of stations is equally good for the three earthquakes, it is expected that the slip distribution will be reliably obtained for the other two earthquakes. The fact that the final models for the three earthquakes well explained the geodetic data also indicates the validity of slip distribution.

The solutions for rupture propagation pattern are less stable when compared with the slip distribution. The present results

show, however, that the initiating point of rupture generally coincided with the hypocenter determined from the travel time analysis.

In Table 1, the fault parameters obtained for the final models of the three earthquakes are summarized. The total seismic moments of these three earthquakes are almost the same. However, the rupture processes are fairly different from each other.

In Fig. 21, the slip distribution is again compared with the aftershock distribution for each of the three earthquakes. We notice that only few aftershocks occur in the region of large slip. Most of large aftershocks took place near the edge of the large slip region and in the region of small slip. Similar results have been obtained by many authors (e.g. Doser and Kanamori, 1986; Mendoza and Hartzell, 1988). The results are consistent with the following interpretation (e.g. Aki, 1979; Mendoza and Hartzell, 1988). In the large-slip region, stresses are released by the main shock faulting, while the stresses increase in the surrounding regions, and cause aftershocks. These stress changes are confirmed by numerical experiments of dynamic fault rupture (e.g. Mikumo and Miyatake, 1978).

Using the kinematic inversion models obtained in this paper with some reference to the recent results of estimating dynamic parameters (Miyatake et al., 1991a,b; Mikumo et al., 1991), we discuss the dynamic rupture processes of the three earthquakes in detail. The dinamic parameters to be estimated are the dynamic stress drop and the strength excess over the fault. The strength excess $\sigma_S - \sigma_0$, which is defined by Quin (1990), is the difference

between the peak stress (static strength) σ_s and the initial shear stress σ_0 . The strength excess is a good indication of strength (Das and Aki, 1977), although it depends on the grid-size used in numerical calculations and hence its absolute value cannot be discussed.

We estimate these dynamic parameters by the following procedure (Mikumo and Miyatake, 1991). The dynamic rupture process is reconstructed by using a three-dimensional spontaneous shear crack model. The equations of motion in a horizontally layered half space are solved by a finite difference method (FDM). Smoothing the kinematic inversion model, the fault slip and the rupture time at each fault segment for the FDM grid are obtained. These rupture times are used as a fracture criterion for dynamic rupture propagation instead of the conventional critical stress criterion. Each fault segment is locked until the estimated rupture time t_r and is ruptured with a given stress drop at $t=t_r$. The static shear strength σ_s for each fault segment is estimated from the peak stress just before the rupture. Because the initial stress σ_0 cannot be determined by our analysis, only the strength excess can be estimated.

For the fixed rupture times, the final slips depend only on the dynamic stress drop (Quin, 1990). To estimate the distribution of dynamic stress drop, varying it successivly, we calculate the dynamic fault slips and compared them with the corresponding slips from kinematic inversion. Calculations are repeated for several times until a best fit is obtained btween the dynamic and kinematic slips. Miyatake (1991) proposed a simple method to

estimate the distribution of stress drop. He calculated the distribution of static stress drop by solving the equibrium equation with boundary conditions of the slip distribution on the fault plane and used it as the distribution of dynamic one, assuming that the difference btween static and dynamic stress drop is not significant.

For two vertical strike-slip faults, the NaganoKen-Seibu earthquake and the GifuKen-Chubu earthquake, the method employed by Miyatake (1991) was used. For the case of a dipping fault, Mikumo and Miyatake (1991) developed a method and applied it to the Kita-Mino earthquake.

Figure 22 shows the resulting stress drop and strength excess for the three earthquakes analyzed in this paper. As shown in Fig. 22, the distribution of both the stress drop and strength excess are heterogeneous over the fault for all the three earthquakes. The ratio of the strength excess to the stress drop is a parameter indicating rupture characteristics. In the region with small values of this parameter, the rupture may be regarded as an asperity type, whereas in the region with their large values, the rupture is of a barrier type.

In the case of the NaganoKen-Seibu earthquake, two high stress drop regions exist at shallow depth in the western and eastern parts of the fault, corresponding to large slip areas. In the eastern, high stress drop region the strength excess is also high, while it is low in the western, high stress drop region. On the other hand, the deeper part of the fault shows low stress drop with high strength excess. The above results suggest that

the rupture initiated from a small zone with low strength (asperity) at a shallow depth and spread over the fault, and that it was arrested by high strength barriers in the deep and western sections. In the eastern part of the fault, large stress drop occurred, in spite of the high strength. Most of aftershocks occurred at the deeper part of the fault which is considered to be a barrier zone, where the strength excess is high and the stress drop is low.

For the GifuKen-Chubu earthquake, a high stress drop region spreads over the deeper part of the fault extending northwestward to shallower depths. A high stress drop region is also located separately at a mid-depth in the southeastern part of the fault, and high strength excess is seen in the northwestern part. The results indicated that the rupture initiated at the central shallow part of the fault with low stress drop and low strength, and propagated mainly downward through a channel with low strength excess. The rupture was once arrested by the high strength excess area at the northwestern mid-depth, then propagated with high stress drop. Many aftershocks occurred in the southeastern shallow part of the fault where both stress drop and strength excess are low.

In the case of the 1961 Kita-Mino earthquake, high stress drop regions are distributed over the deeper part and in the northwestern shallow part of the fault. Strength excess is high in the southeastern deep and shallow parts of the fault. The rupture started from a zone with low strength excess (asperity) and propagated to the center of the fault quite smoothly. Then

the rupture was decelerated by the high strength excess regions located at the central deep part and southwestern shallow part of the fault. Aftershocks are concentrated around a barrier in the southwestern shallow part where the strength excess is high and the stress drop is low.

At the initial stage of faulting, the rupture is of an asperity-break type, and then both the asperity and the barrier type rupturing occurred at later stages for all three earthquakes. It should be mentioned, however, that the overall rupture processes of the three earthquakes are very different.

We compare the present results with those for two earthquakes in the Izu region, the 1974 Izu-Hanto-Oki earthquake and the 1980 Izu-Hanto-Toho-Oki earthquake (Miyatake et al., 1991a,b). These two earthquake show relatively simple rupture processes, and it appears that high stress drop zones and high strength excess zones are distributed complimentally. In these two earthquakes, the rupture initiated from a small zone in the asperity region with high stress drop and low strength excess, propagated to barriers with high strength excess and low stress drop, and then stopped. This simple process contrasts sharply to more complicated processes of the earthquakes in the Chubu district.

Other major difference between earthquakes in the Chubu district and in the Izu region is the location of high stress drop zones. The stress drop is low at the shallow part of the faults for the two Izu earthquakes, while there exists a high stress drop region at shallow depths for the three earthquakes in the Chubu district. The zones of high strength excess are also

distributed at the shallow part. This difference leads to the following possible interpretation. In the Izu region, the shallow part of the fault cannot accumulate large strains because of low strength. The stresses are released seismically and/or aseismically before main shock faulting. In the northwestern part of the Chubu district, on the other hand, the shallow part of the fault as well as the deeper part could accumulate strains and break with high stress drop during the main shock. The high strength of the shallow part of the fault could cause the rupture initiating at shallow depths.

The above features suggest that the properties of the shallow crust in the Chubu region may be more heterogeneous, with higher frictional strength in pre-existing fault surfaces, than those in the Izu region.

5. Conclusions

The rupture processes of three inland earthquakes that occurred in the northwestern Chubu district, in central Japan, have been investigated here by the inversion of the observed strong motion waveforms. Then the dynamic rupture models reconstructed from the kinematic inversion models have been discussed. The main conclusions are as follows:

(1) The inversion results indicate that the slip distribution on the fault is considerably heterogeneous over the fault for all the three earthquakes. The rupture processes of these earthquakes are fairly different from each other.

(2) It is the common feature of the earthquakes that only a few aftershocks occurred in the region of large slip and that most large aftershocks took place near the edge of the large slip region and in the region of small slip.

(3) The distribution of the stress drop and strength excess are extremely heterogeneous over the fault plane and their pattern is different in the three earthquakes.

(4) The dynamic models of these three earthquakes show complicated rupture patterns. At the initial stage of faulting, the rupture is of an asperity-break type, and then both the asperity and the barrier type rupturing occurred at later stages.

(5) The rupture processes of the three earthquakes in the Chubu region are more complicated than those of earthquakes in the Izu region. Also, there exists a high stress drop zone at shallow depth for the earthquakes in the Chubu region, whereas the stress drop is low at the shallow part of the fault for the

two Izu earthquakes.

Acknowledgments

I am grateful to Prof. Takeshi Mikumo for critical reading of the manuscript and encouragement. I thank Dr. Minoru Takeo for useful discussion and encouragement. I thank also Dr. Takashi Miyatake for kindly sending preprints and valuable suggestions. I am grateful to Dr. Kazuro Hirahara for useful comments and encouragement. My thanks are also due to the staff members of Seismological Observatory for their encouragement. I am grateful to the staff members of Japan Meteorological Agency stations for providing me the strong motion seismograms. The inversion program of SALS (Statistical Analysis with Least-squares fitting) was used in this study. Computations were carried out on a HITAC M-280H and S-810 at Meteorological Research Institute and FACOM A-400 at Seismological Observatory.

References

Aki, K., 1979, Characterization of barriers on an earthquake fault, J. Geophys. Res., 84, 6140-6148.

Alekseev, A.S. and B.G. Mikhailenko, 1980, Solution of dynamic problems of elastic wave propagation in inhomogeneous media by a combination of partial separation of variables and finite difference method, J. Geophys., 48, 161-172.

Archuleta, R.J., 1976, A faulting model for the 1979 Imperial Valley earthquake, J. Geophys. Res., 89, 4559-4585.

Bouchon, M., 1981, A simple method to calculate Green's functions for elastic layered media, Bull. Seism. Soc. Am., 71, 959-971.

Das, S. and K. Aki, 1977, Fault plane with barriers: A versatile earthquake model, J. Geophys. Res., 82, 5648-5670.

Doser, D.I. and H. Kanamori, 1986, Depth of seismicity in the Imperial Valley region (1977-1983) and its relationship to heat flow, crustal structure, and the October 15, 1979, earthquake, J. Geophys. Res., 91, 675-688.

Fukuyama, E. and K. Irikura, 1986, Rupture process of the 1983 Japan Sea (Akita-Oki) earthquake using a waveform inversion method, Bull. Seism. Soc. Am., 76, 1923-1940.

Fukuyama, E. and T. Mikumo, 1991, Dynamic rupture analysis: Inversion for the Source process of the 1990 Izu-Oshima, Japan, earthquake(M6.5), submitted to J. Geophys. Res.

Hamada, N., 1987, Re-examination of seismicity associated with destructive inland earthquakes of Japan and its seismological

significance, Pap. Meteor. Geophys., 38, 77-156, (in Japanese).

Hartzell, S. H. and T. H. Heaton, 1983, Inversion of strong grand motion and teleseismic waveform data for the fault rupture history of the 1979 Imperial Valley, California, earthquake, Bull. Seis. Soc. Am., 73, 1553-1583.

Haskell, N.,1969, Elastic displacements in the near-field of a propagating fault, Bull. Seism. Soc. Am., 59, 865-908.

Ichikawa, M., 1971, Reanalysis of mechanisms of earthquakes occurred in and near Japan, and statistical studies of nodal plane solutions obtained, 1926-1968. Geophys. Mag., 35,207-274.

Iida, M., T. Miyatake and K. Shimazaki, 1990, Relationship between strong-motion array parameters and the accuracy of source inversion and physical waves, Bull. Seism. Soc. Am., 80, 1533-1552.

Japan Meteorological Agency, 1986, Report on the NaganoKen-Seibu earthquake, 1984, Tech. Rep. Japan Meteorol. Agency, 107, 1-46, (in Japanese).

Kanamori, H., 1972, Determination of effective tectonic stress associated with earthquake faulting the Tottori earthquake of 1943, Phys. Earth Planet. Inter., 5, 426-434.

Kanamori, H., 1981, The nature of seismicity before large earthquakes, in "Earthquake prediction, an International Review. M. Ewing Ser. 4, ed. D. Simpson and P. Rechards, American Geophysical Union".

Kawasaki, I., 1975, The focal process of the Kita-Mino earthquake of August 19, 1961, and its relationship to a quaternary fault, the Hatogayu-Koike fault, J. Phys. Earth, 24, 227-250.

Kennet, L.N. and N. J. Kerry, 1979, Seismic waves in a stratified half space, Geophys. J. R. Astr. Soc., 57, 557-583.

Kikuchi, M. and Y. Fukao, 1985, Iterative decomvolution of complex body waves from great earthquakes -the Tokachi-Oki earthquake of 1968, Phys. Earth Planet. Inter., 37, 235-248.

Mendoza, C. and S.H. Hartzell, 1988, Aftershock patterns and main shock faulting, Bull. Seism. Soc. Amer., 78, 1438-1449.

Mikumo, T., 1973, Faulting mechanism of the Gifu earthquake of September 9, 1969 and some related problems, J. Phys. Earth, 21, 191-212.

Mikumo, T., K. Hirahara and T. Miyatake, 1987, Dynamic fault rupture processes in heterogeneous media, Tectonophysics, 144 19-36.

Mikumo, T. and T. Miyatake, 1978, Dynamical rupture process on a three-dimensional fault with non-uniform frictions and near-field seismic waves, Geophys. J. R. Astr. Soc., 54, 417-438.

Mikumo, T. and T. Miyatake, 1991, Dynamic rupture process on a dipping fault, and estimates of dynamic stress drop and strength excess from the results of waveform inversion, submitted to Geophys. J. Int.

Mikumo, T., T. Miyatake and N. Mikami, 1991, Dynamic fault rupture processes recovered from the results of waveform inversion (II) Method and application to thrust faults, Program and Abstracts, Seism. Soc. Japan, 2, 120.(in Japanese).

Miyatake, T., 1991, Reconstruction of dynamic rupture process of an earthquake with constraints of kinematic parameters,

submitted to Geophys. Res. Lett.

Miyatake, T., T. Mikumo and N. Mikami, 1991a, Dynamic fault rupture processes recovered from the results of waveform inversion (I) Method and application to strike-slip faults, Program and Abstracts, Seism. Soc. Japan, 2, 119.(in Japanese).

Miyatake, T., N. Mikami and T. Mikumo, 1991b, Dynamic fault rupture processes recovered from the results of waveform inversion (III) Spatial distributions of asperities and barriers on the faults, Program and Abstracts, Seism. Soc. Japan, 2, 121.(in Japanese).

Mori, J. and K. Shimazaki, 1985, Inversion of intermediate-period Rayleigh waves for source characteristics of the 1968 Tokachi-Oki earthquake, J. Geophys. Res., 90, 11374-11382.

Olson, A.H., 1982, Forward simulation and linear inversion of earthquake ground motion, Ph. D. thesis, Univ. California, San Diego.

Olson, A.H. and Aspel, R.H., 1982, Finite faults and inverse theory with application to the 1979 Imperial Valley earthquake, Bull. Seism. Soc. Am., 72, 1-14.

Quin, H., 1990, Dynamic stress drop and rupture dynamics of the October 15, 1979 Imperial Valley, California, earthquake, Tectonophysics, 175, 83-117.

Research Group for Active Faults of Japan, 1991, Active Faults in Japan: Sheet Maps and Inventories (revised edition), Univ. Tokyo Press, Tokyo, 437pp. (in Japanese).

Sato, R. and M. Matsu'ura, 1974, Strains and tilts on the surface of a semi-infinite medium, J. Phys. Earth, 22, 52-57.

Takeo, M., 1985,Near-field synthetic seismograms taking into account the effects of anelasticity -The effects of anelastic attenuation on seismograms caused by a sedimentary layer-, Pap. Meteorol. Geophys., 36, 245-257.(in Japanese).

Takeo, M., 1987, An inversion method to analyze the rupture processes of earthquakes using near-field seismograms, Bull. Seism. Soc. Am., 78, 1074-1091.

Takeo, M. and N. Mikami, 1987, Inversion of strong motion seismograms for the source process of the NaganoKen-Seibu earthquake of 1984, Tectonophysics, 144, 271-285.

Takeo, M. and N. Mikami, 1990, Fault heterogeneity of inland earthquakes in Japan, Bull. Earthq. Res. Inst., 65, 541-569.

Watanabe, H. and A. Kuroiso, 1970, Aftershock of earthquake of the Central part of Gifu Prefecture, September 9, 1969, Bull. Earthq. Res. Inst., 48, 1195-1208.(in Japanese).

Yamashina, K. and T. Tada, 1986, A fault model of the 1984 Western Nagano Prefecture earthquake based on the distance change of trilateration points, Bull. Earthq. Res. Inst., 60, 221-230.(in Japanese).

Yoshida S. and K. Koketsu, 1990, Simultaneous inversion of waveform and geodetic data for the rupture process of the 1984 Naganoken-Seibu, Japan, earthquake, Geophys. J. Int., 103, 355-362.

Figure captions

Fig. 1. Epicenters of the three earthquakes analyzed in this study and the distribution of active Quaternary faults (after Research Group for Active faults of Japan, 1991). a: the 1984 NaganoKen-Seibu earthquake, b: the 1969 GifuKen-Chubu earthquake, c: the 1961 Kita-Mino earthquake.

Fig. 2. Models of the velocity structure used for calculation of Green's functions. For Structure B, attenuation structure for P and S are also assumed.

Fig. 3. Locations of the 1984 NaganoKen-Seibu earthquake and the stations used in this study.

Fig. 4. Focal mechanisms of a foreshock and the main shock (lower hemisphere, equal-area projections) of the 1984 NaganoKen-Seibu earthquake. Solid and open circles indicate compressional and dilatational initial motions respectively.

Fig. 5. Arrangement of subfaults plotted on a cross section of the distribution of aftershocks which occurred before the largest aftershock. This cross section was supplied by the Japan Meteorological Agency (1986). The main shock (a large circle at the central shallow part of the fault) and the the largest aftershock were also plotted on the cross section. Diamonds indicate the center of each subfault.

Fig. 6. Pattern of rupture propagation and the distribution of dislocations on the main shock fault. a. Rupture fronts at every second, inferred from the two inversion solutions. b. Distribution of dislocations.

Fig. 7. Comparison of the strong motion seismograms at IID, TKY, MTM, GIF and MAT with the corresponding synthetic seismograms calculated from model A and model B.

Fig. 8. Distribution of aftershocks projected on the fault plane of the main shock. The isograms of average dislocation obtained from model A and model B are drawn with solid lines on the fault plane of each model. Broken lines denote the edge of the fault plane inferred from the distribution of dislocations.

Fig. 9. Focal mechanism solution of the 1969 GifuKen-Chubu earthquake (after Mikumo, 1973).

Fig. 10. Arrangement of subfaults and the cross section of aftershock distribution by Hamada (1987). Solid and open circles show the main shock and aftershocks which occurred in September, 1969, respectively.

Fig. 11. Distribution of stations (solid circles) and the fault of the 1969 GifuKen-Chubu earthquake. Large open circle indicates an epicentral distance of 100 km.

Fig. 12. Five different models of rupture processes of the 1969 GifuKen-Chubu earthquake. Distribution of slip is normalized to the average slip in each model (the left panels). Solid and open circles indicate positive and negative slip respectively. Rupture front is shown at every 1 second in the right panel of each model.

Fig. 13. Comparison of the observed seismograms with the corresponding synthetic seismograms obtained from the final model (model d).

Fig. 14. Distribution of slip and pattern of rupture propagation on the fault inferred from the final model (model d). Isograms of the slip are plotted on the cross section of aftershock distribution by Hamada (1987) in the upper panel. Rupture front is shown at every 1 second is shown in the lower panel.

Fig. 15. Focal mechanism of the 1961 Kita-Mino earthquake (after Kawasaki, 1975). Solid and open circles indicate compressional and dilatational initial motions, respectively.

Fig. 16. Arrangement of subfaults and the cross section of aftershock distribution by Hamada (1987). Closed circle indicates the main shock.

Fig. 17. Distribution of stations (circles) and the fault of the

1961 Kita-Mino earthquake.

Fig. 18. Three different models of rupture processes of the 1961 Kita-Mino earthquake.

Fig. 19. Comparison of the observed seismograms and the corresponding synthetic seismograms calculated from the final model (model a).

Fig. 20. Distribution of slip and behavior of rupture propagation on the fault inferred from the final model (model a).

Fig. 21 Distribution of fault slips and aftershocks for each of the three inland earthquakes.

Fig. 22. Distribution of stress drop (upper) and strength excess (lower) for the three earthquakes, which have been inferred from the inversion results (Miyatake et al., 1991a,b; Mikumo et al., 1991).

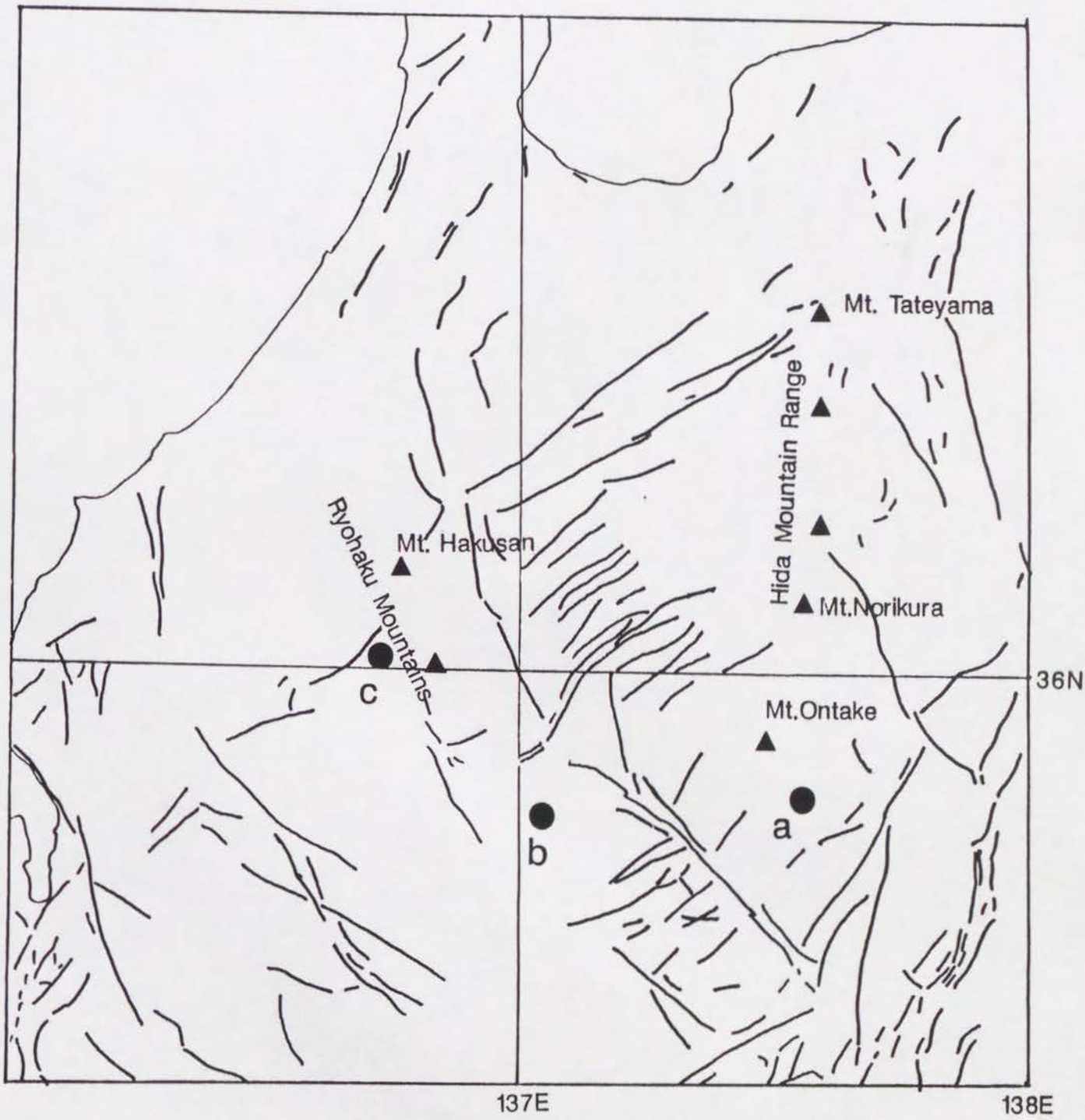
Mt. Tateyama
Hida Mountain Range
Mt. Hakusan
Ryohaku Mountains
Mt.Norikura
36N
Mt.Ontake
a
b
c
137E
138E

Fig. 1

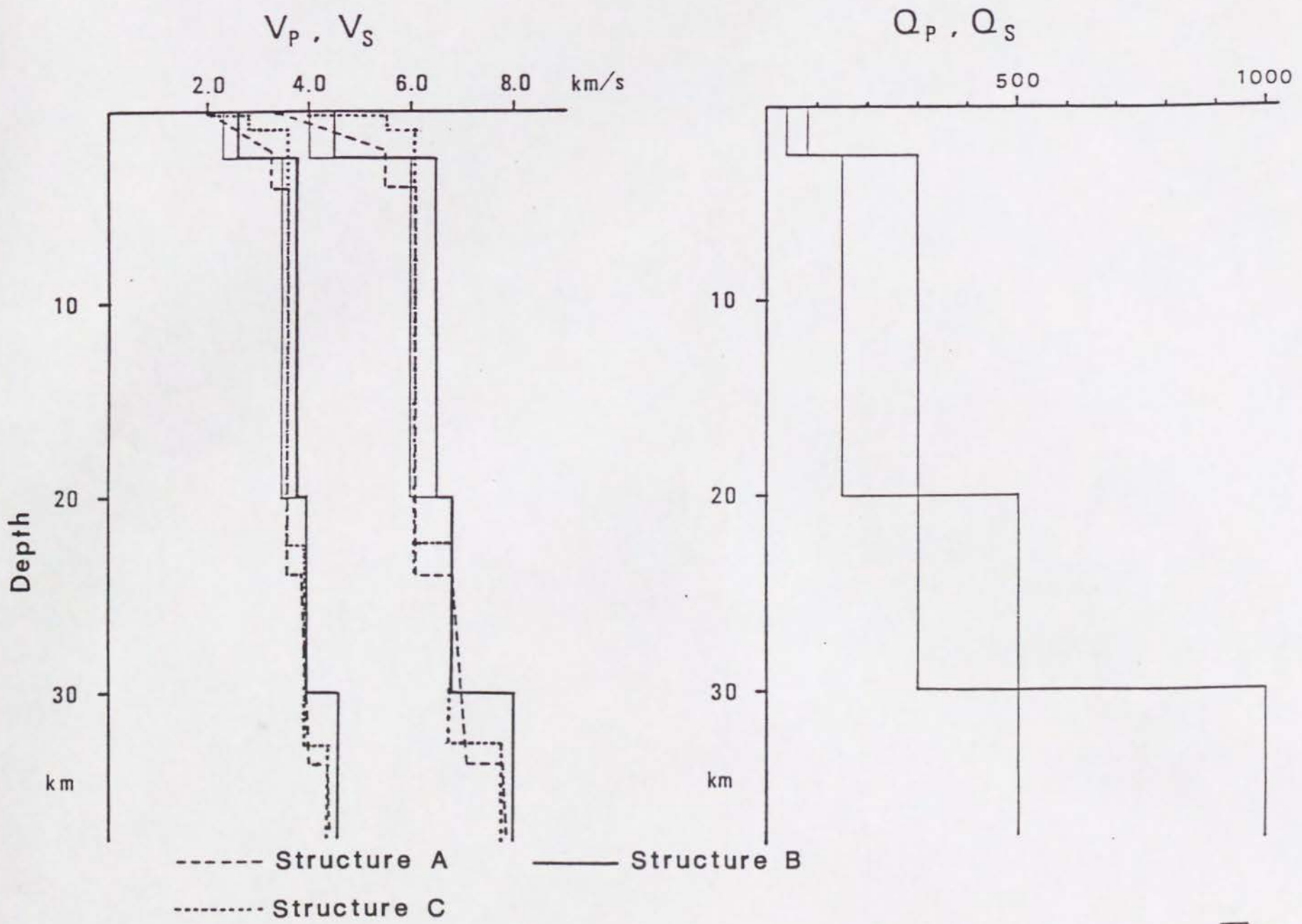
V_P , V_S
2.0
4.0
6.0
8.0
km/s
10
20
30
Depth
km
Q_P , Q_S
500
1000
10
20
30
km
------ Structure A
—— Structure B
--------- Structure C

Fig. 2

Fig. 3

a. foreshock

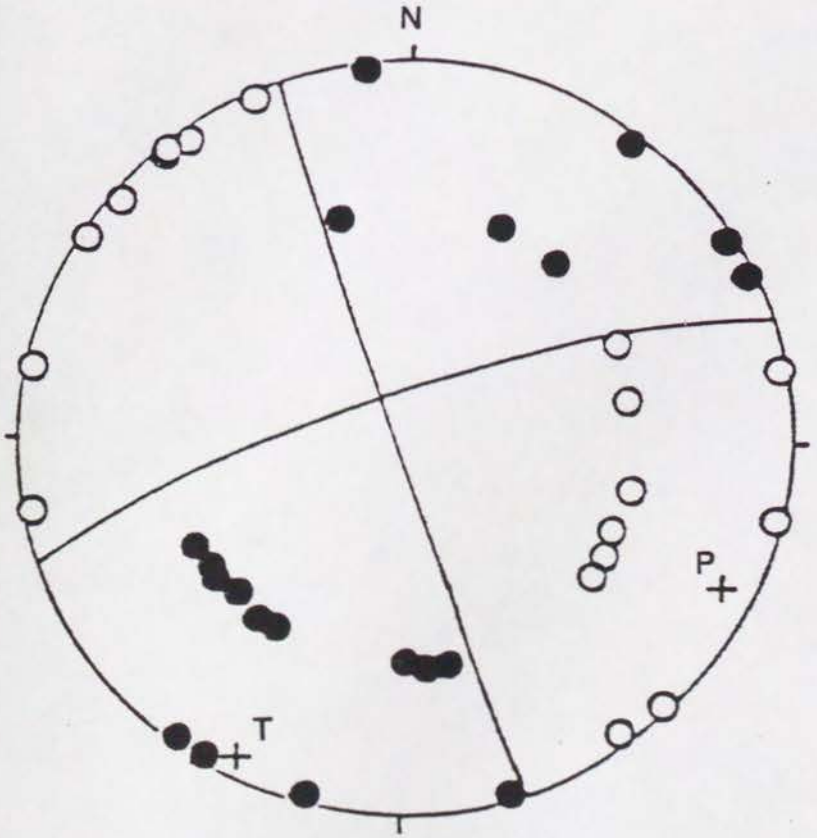

b. main shock

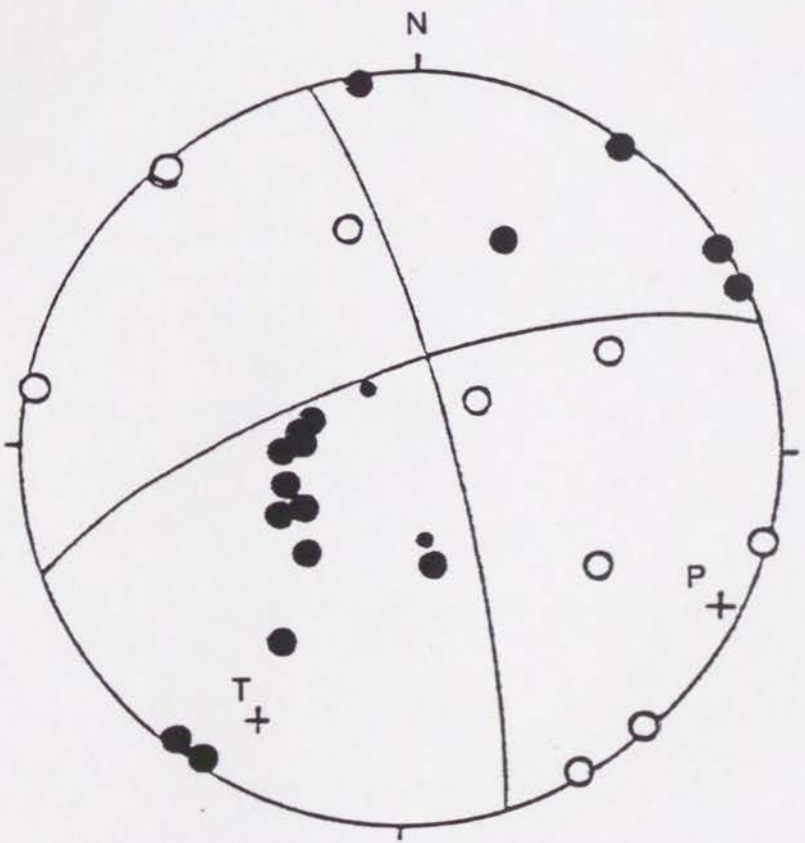

Fig. 4

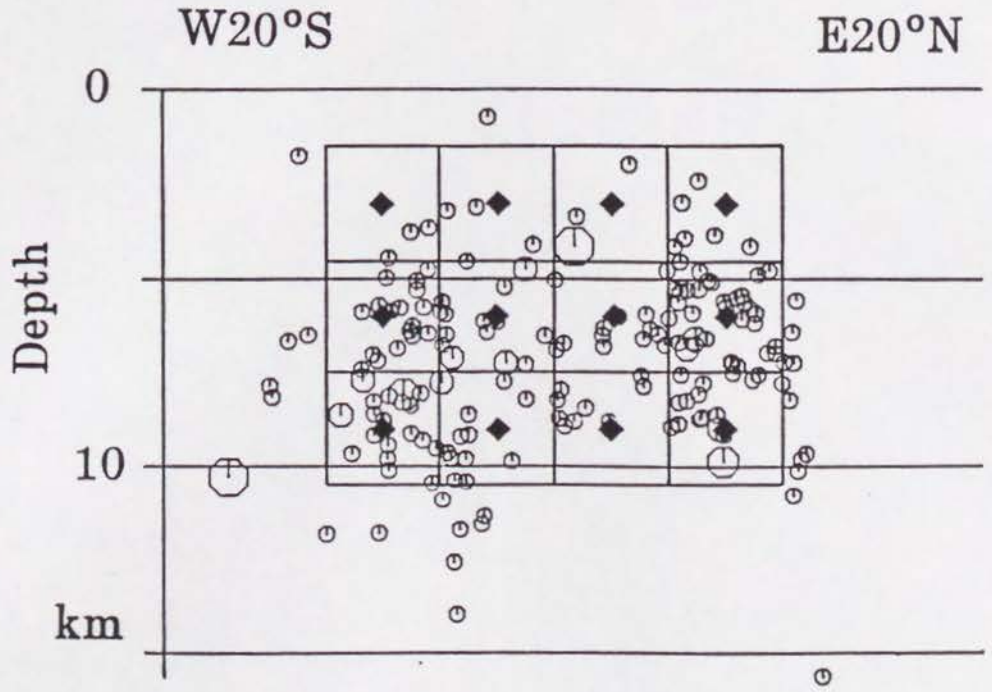

Fig. 5

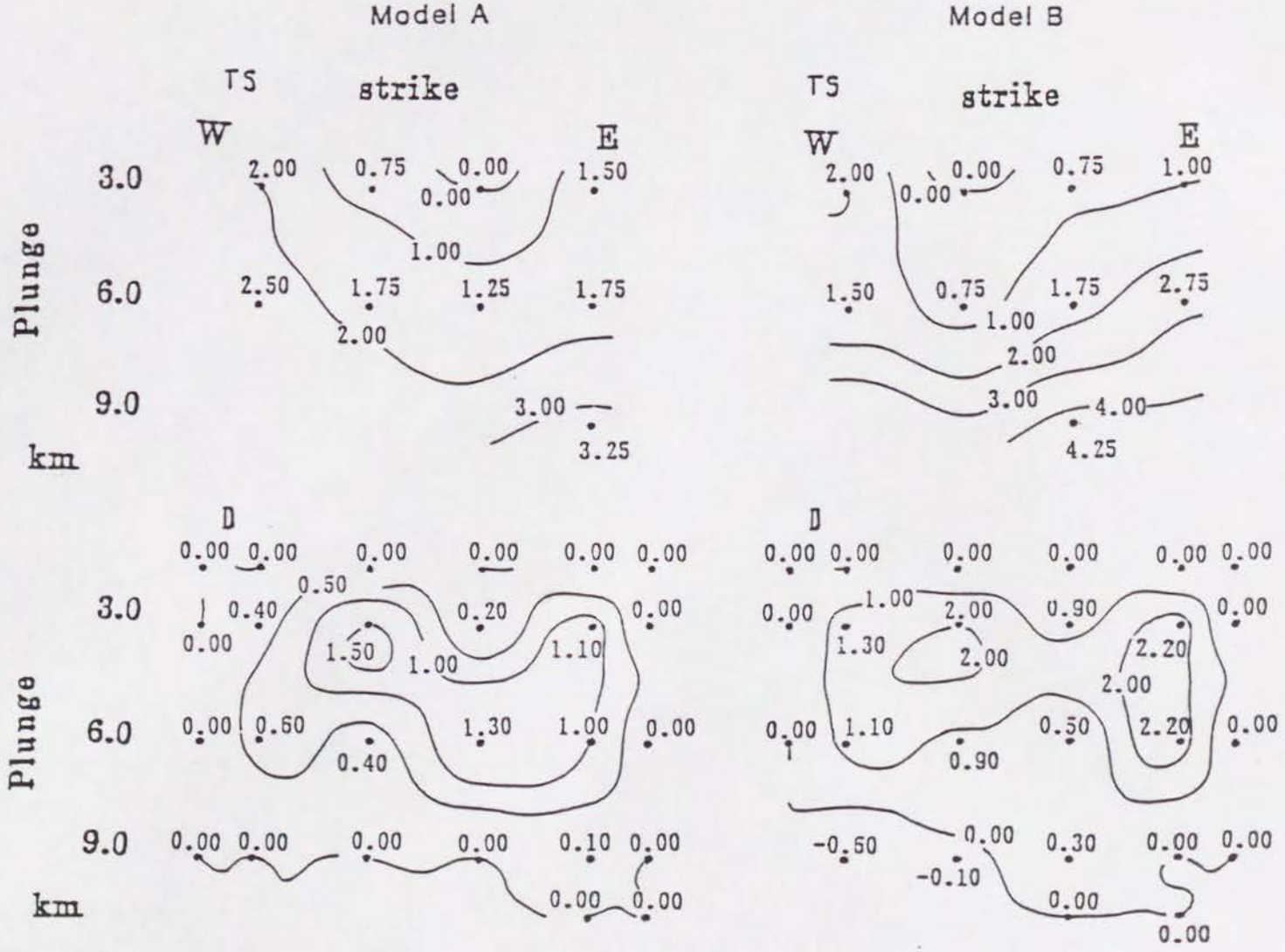
Model A
Model B
TS
strike
W
E
Plunge
3.0
6.0
9.0
km
2.00
0.75
0.00
1.50
0.00
1.00
2.50
1.75
1.25
1.75
2.00
3.00
3.25
0.00
1.00
0.75
1.00
1.50
0.75
1.75
2.75
1.00
2.00
3.00
4.00
4.25
D
0.00
0.50
0.40
0.20
0.00
1.50
1.00
1.10
0.60
1.30
0.40
0.10
1.00
2.00
0.90
1.30
2.20
1.10
0.50
0.90
-0.50
0.30
-0.10

Fig. 6

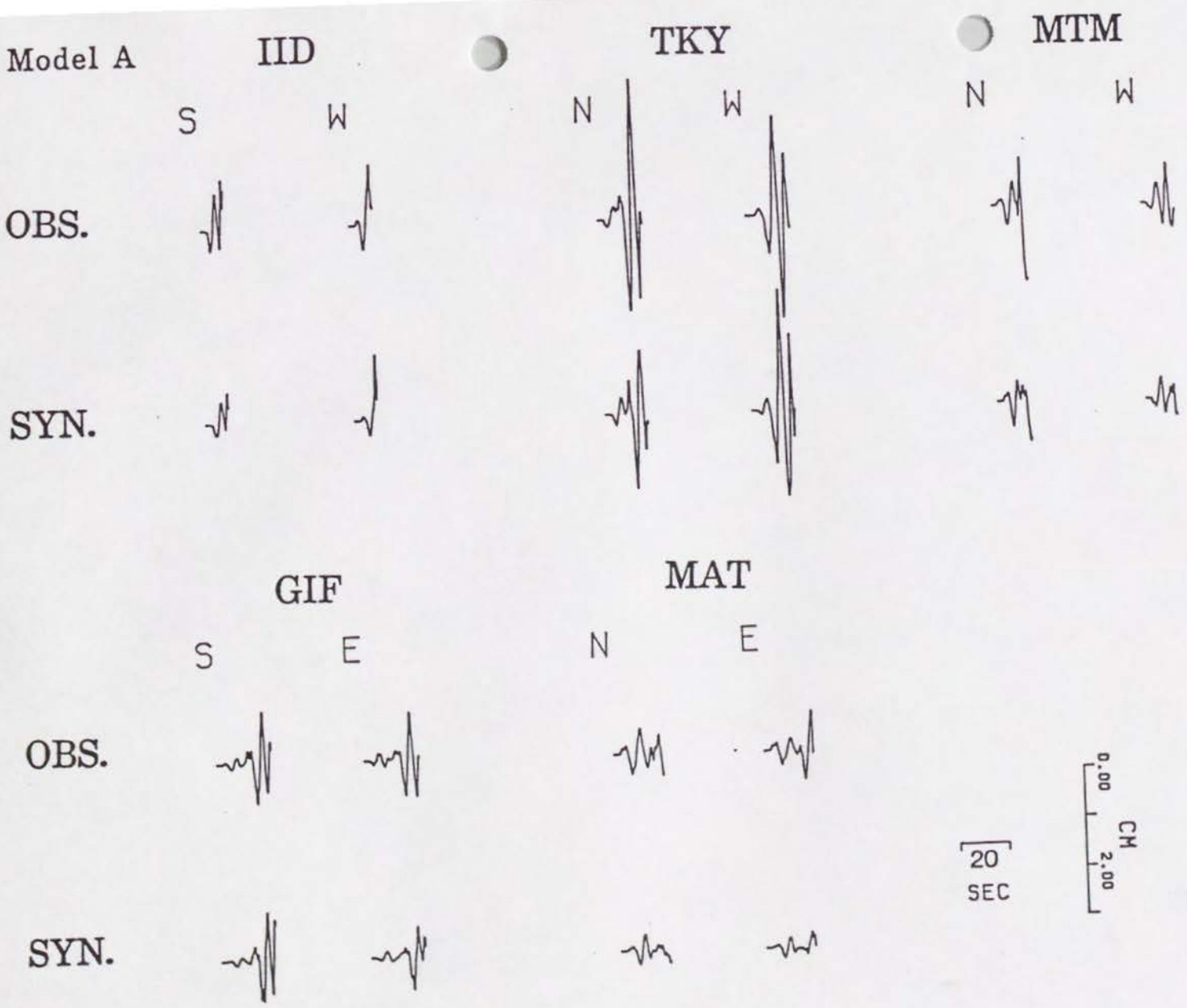
Model A
IID
S
W
OBS.
SYN.
TKY
N
W
MTM
N
W
GIF
S
E
MAT
N
E
20
SEC
0.00
CM
2.00

Fig. 7-1

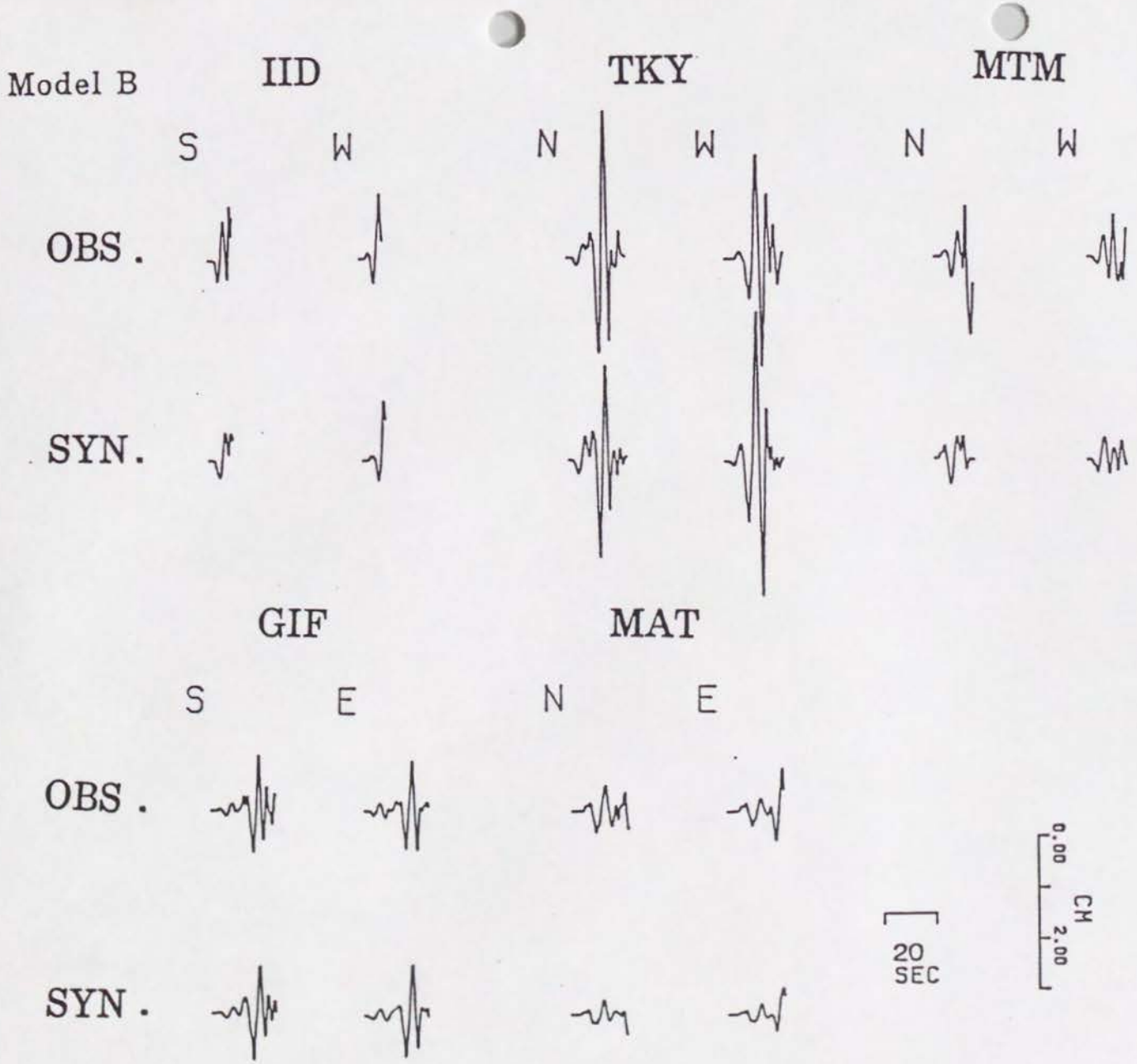
Model B
IID
TKY
MTM
S
W
N
W
N
W
OBS.
SYN.
GIF
MAT
S
E
N
E
OBS.
SYN.
20
SEC
0.00
2.00
CH

Fig. 7-2

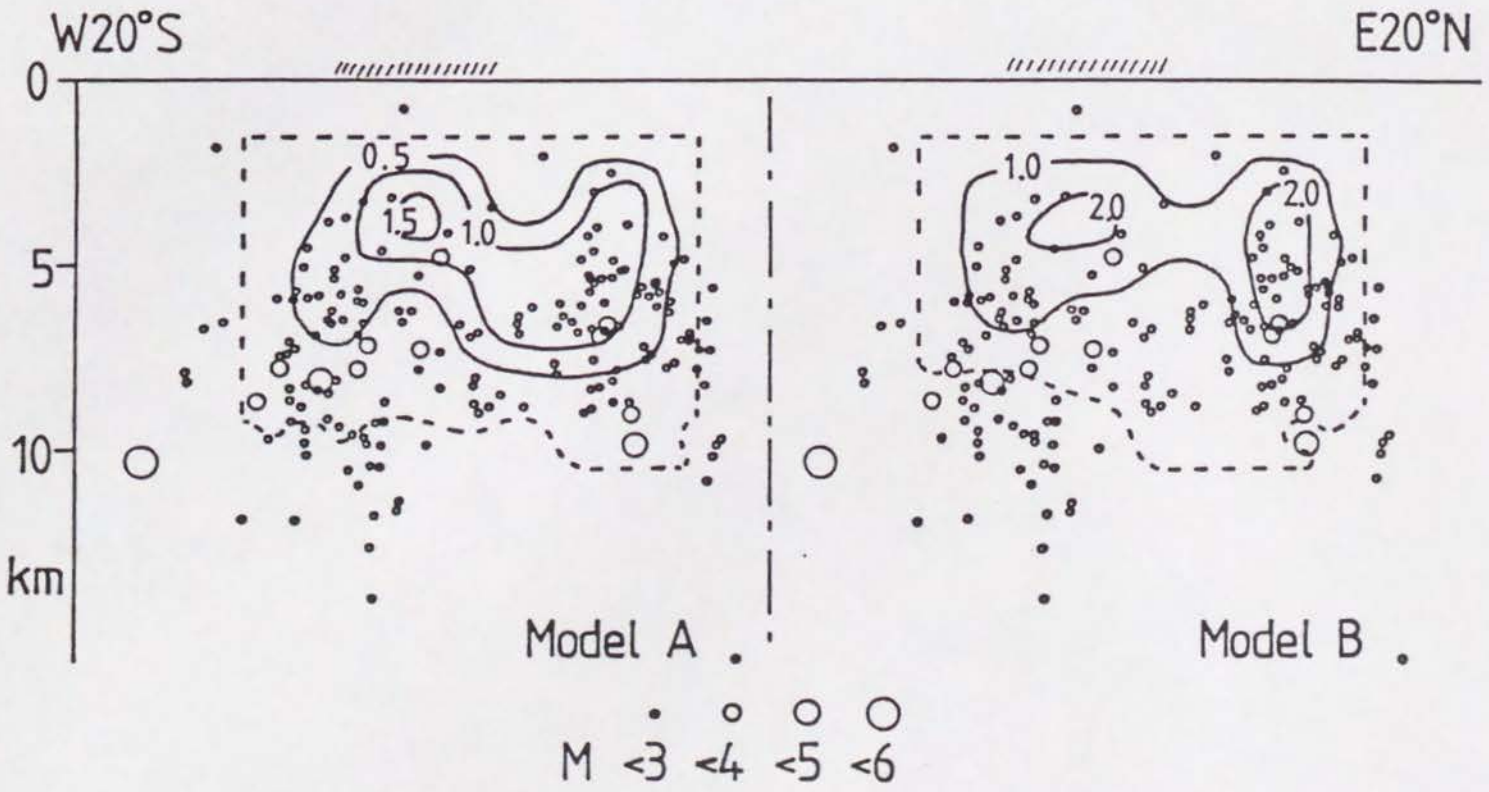

Fig. 8

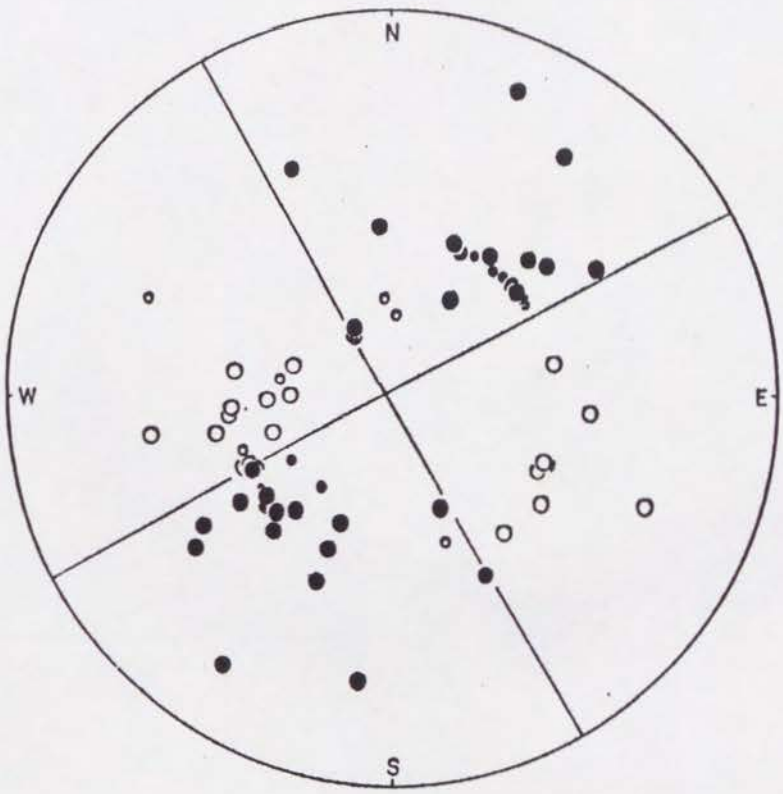

Fig. 9

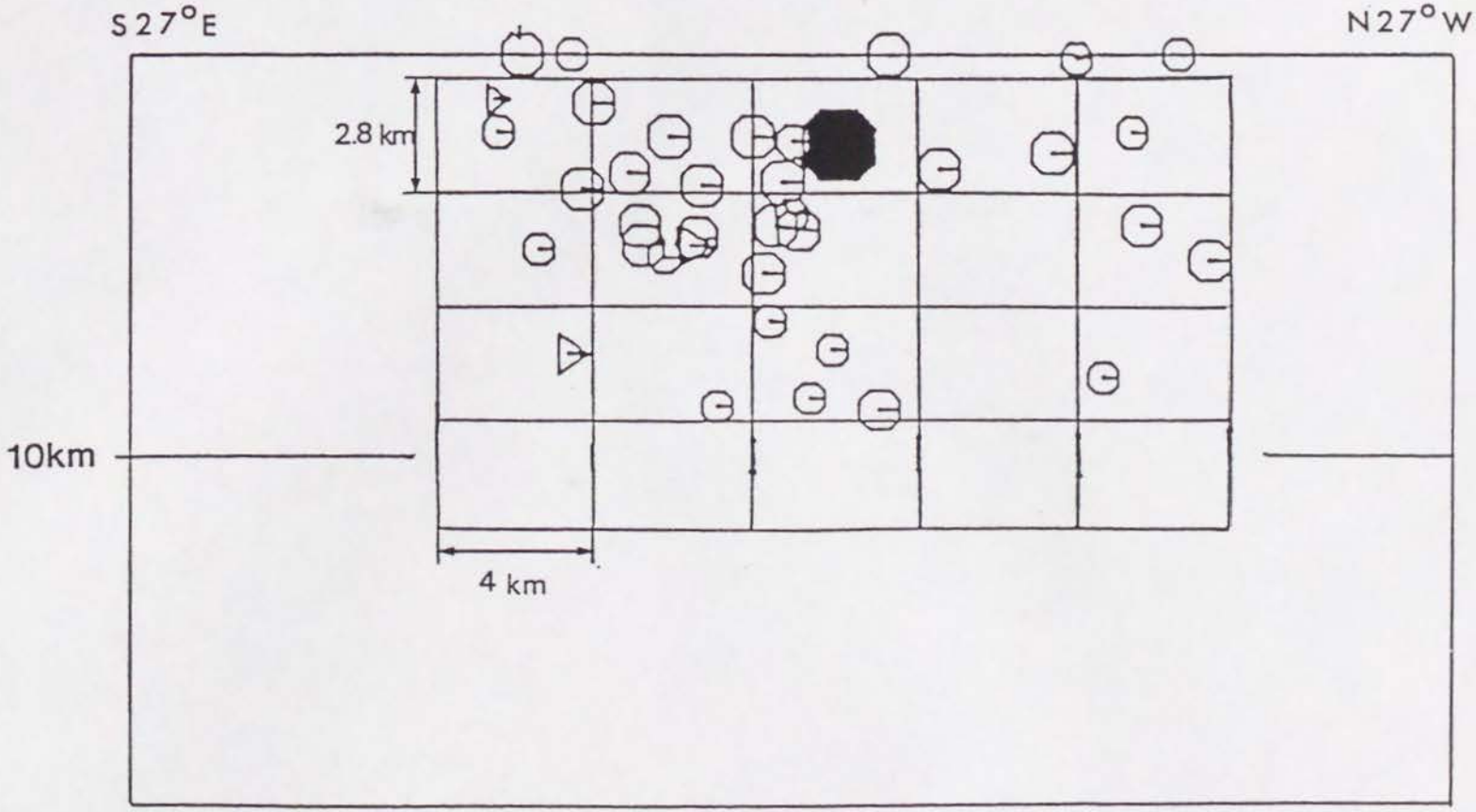

Fig. 10

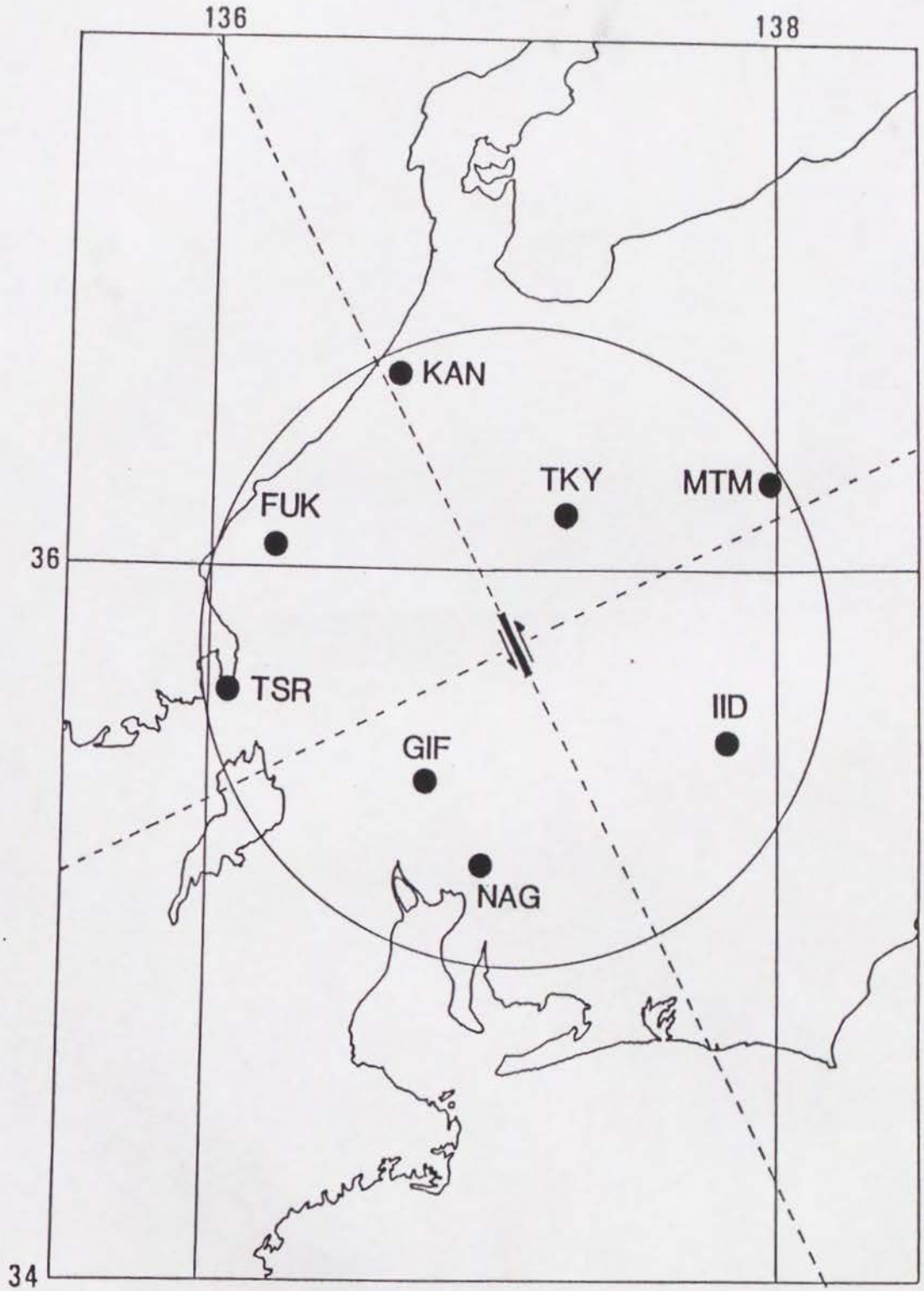

Fig. 11

model a

3 stations
GIF, TKY, IID

Structure C

$M_0 = 7.0 \times 10^{25}$ dyne·cm

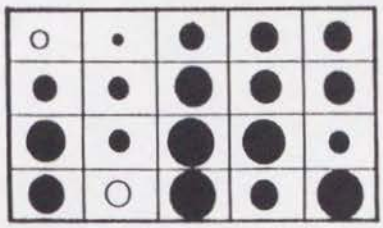

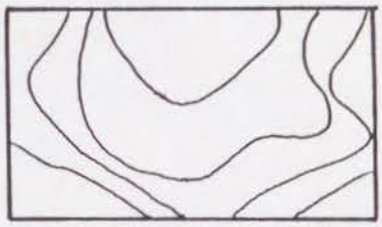

model b

4 stations
NAG, TSR, KAN, MTM

Structure C

$M_0 = 8.9 \times 10^{25}$ dyne·cm

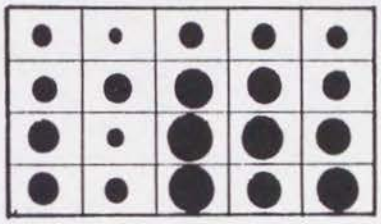

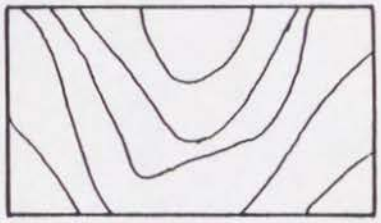

model c

8 stations

Structure C

$M_0 = 5.8 \times 10^{25}$ dyne·cm

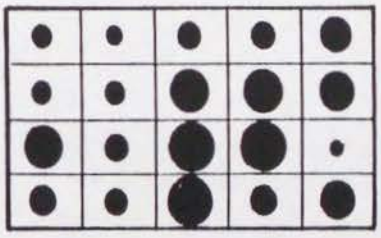

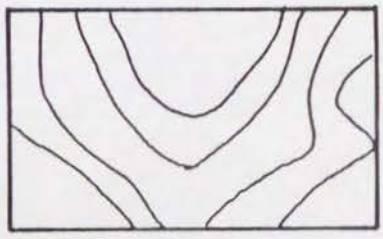

model d

8 stations

Structure A

$M_0 = 5.4 \times 10^{25}$ dyne·cm

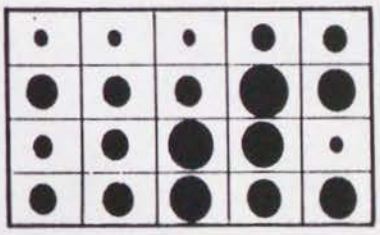

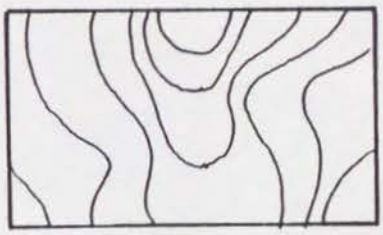

model e

8 stations

Structure A

$M_0 = 3.9 \times 10^{25}$ dyne·cm

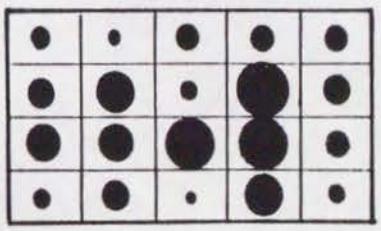

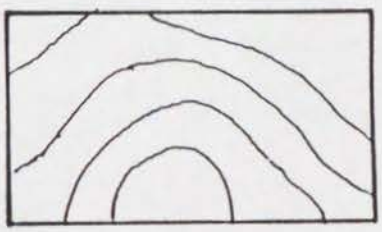

● 2.0 ● 1.0 ● 0.5

Fig. 12

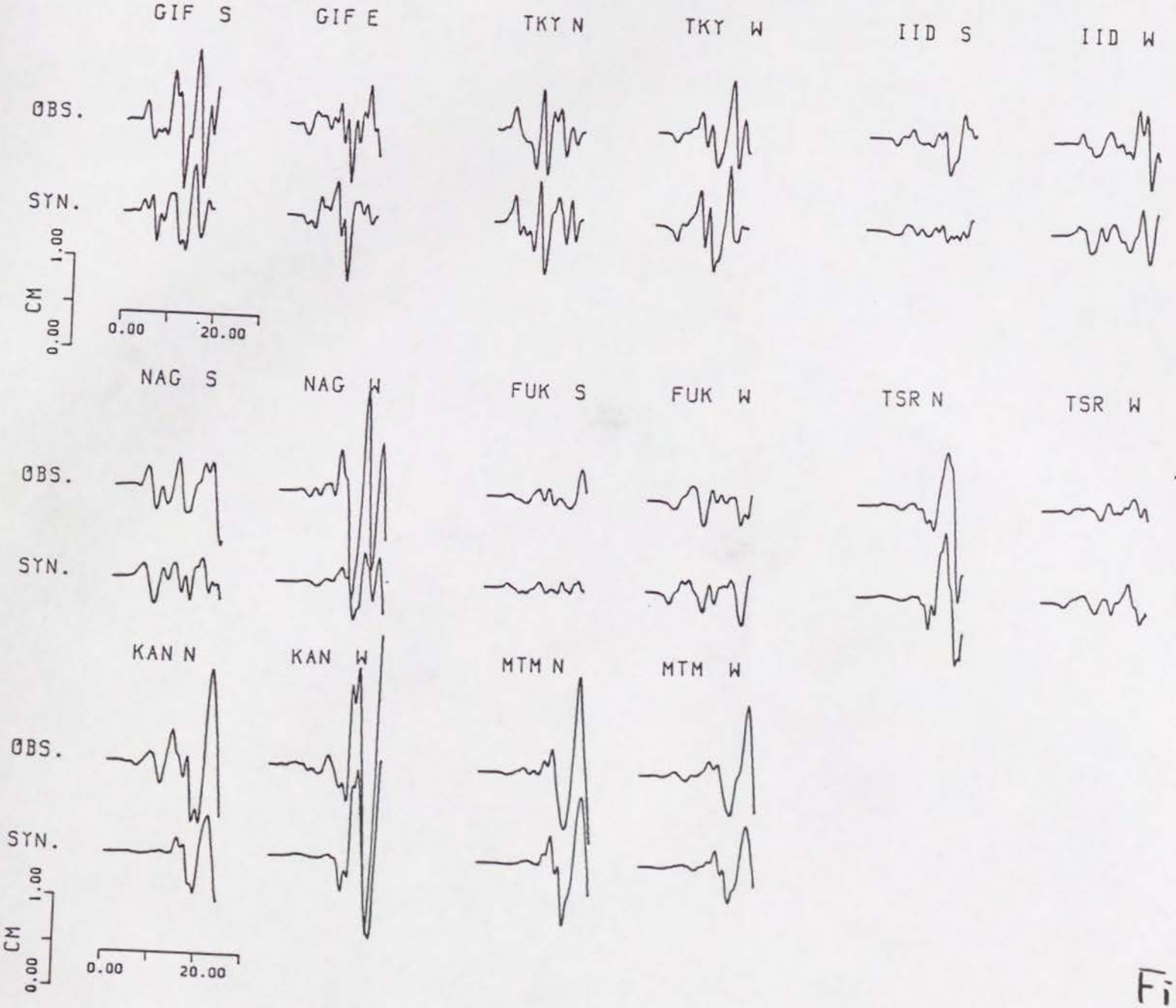
GIF S
GIF E
TKY N
TKY W
IID S
IID W
OBS.
SYN.
CM
1.00
0.00
0.00
20.00
NAG S
NAG W
FUK S
FUK W
TSR N
TSR W
OBS.
SYN.
KAN N
KAN W
MTM N
MTM W
OBS.
SYN.
CM
1.00
0.00
0.00
20.00

Fig. 13

D (m)

0.1	0.1	0.1	0.4	0.3
0.7	0.5	0.5	1.7	1.1
0.2	0.5	1.5	1.4	0.1
0.7	0.6	1.3	0.8	1.0

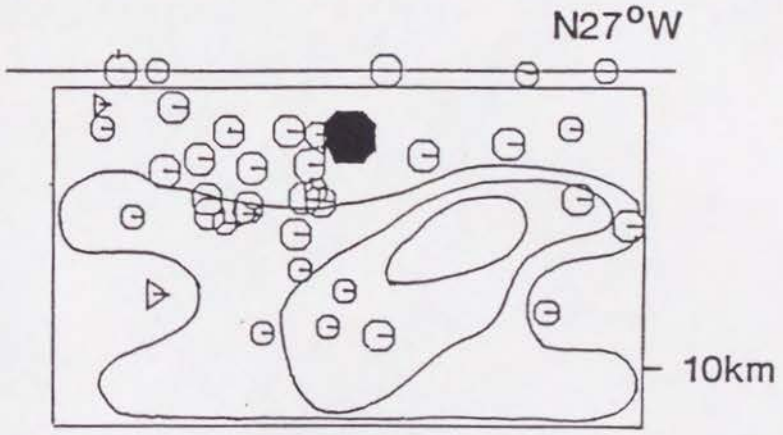

Ts (sec)

4.25	3.0	0.0	1.75	3.75
4.25	3.75	1.5	4.0	5.5
4.75	4.5	2.25	3.5	5.0
5.5	4.0	3.25	3.5	6.0

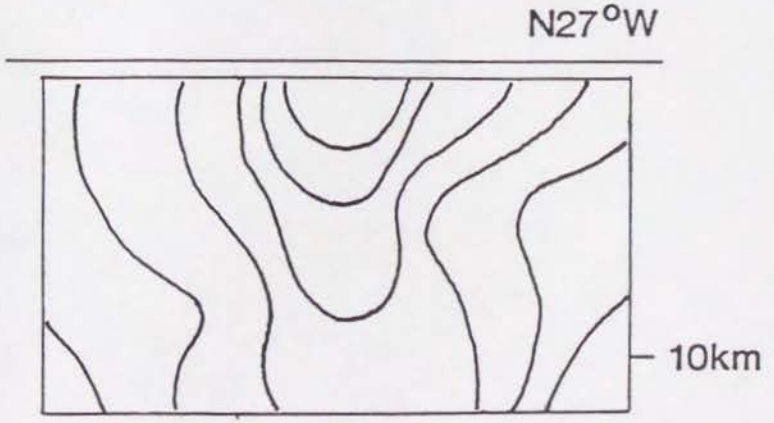

Fig. 14

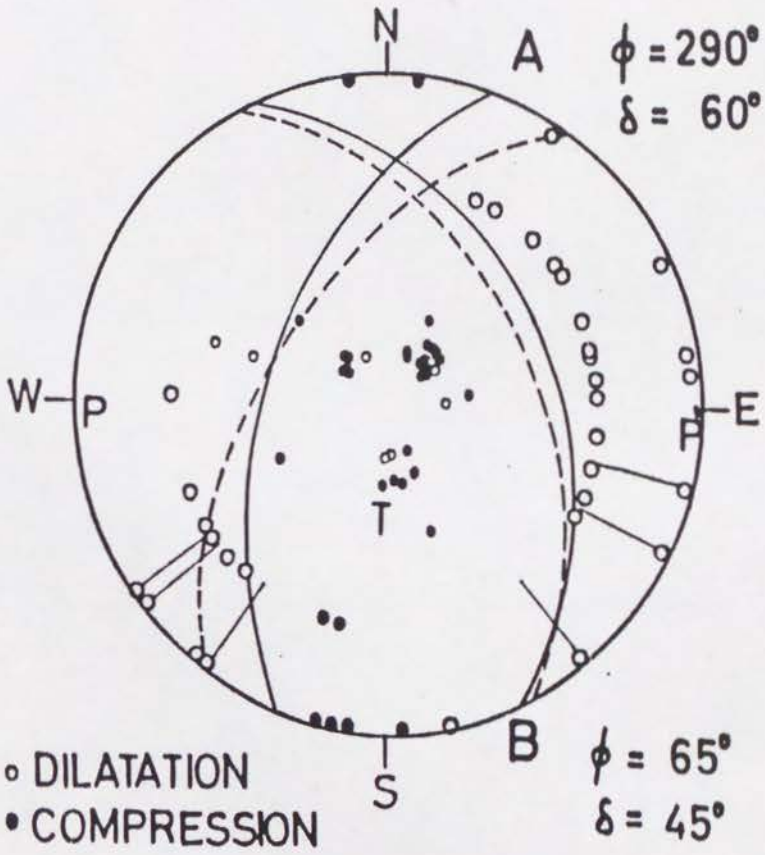

Fig. 15

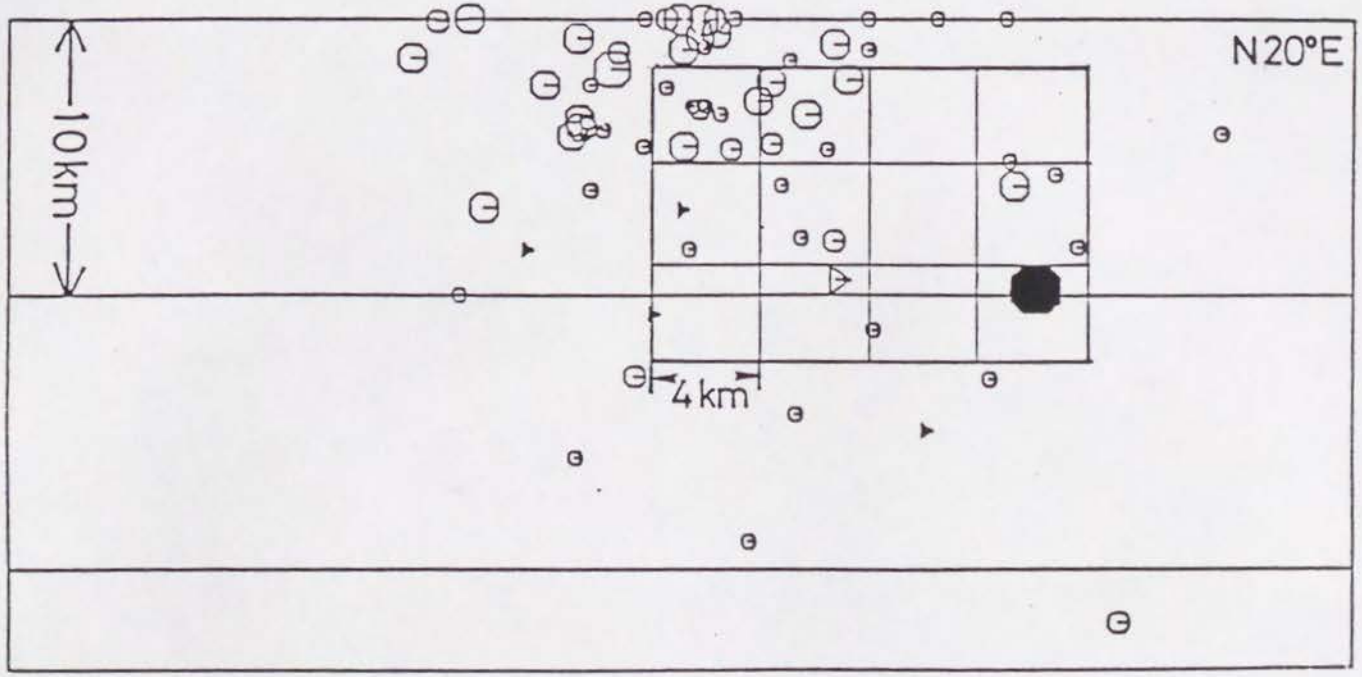

Fig. 16

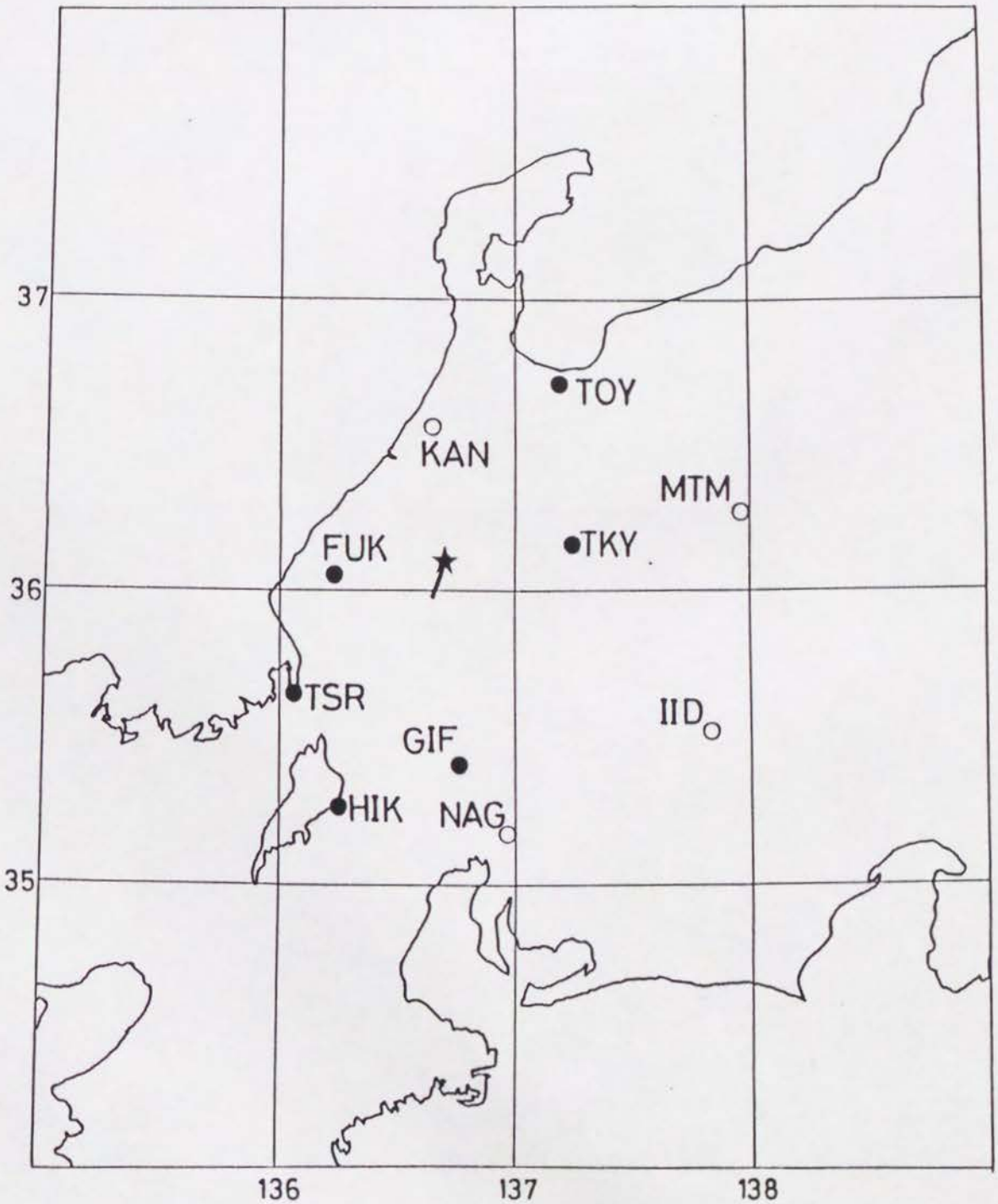

Fig. 17

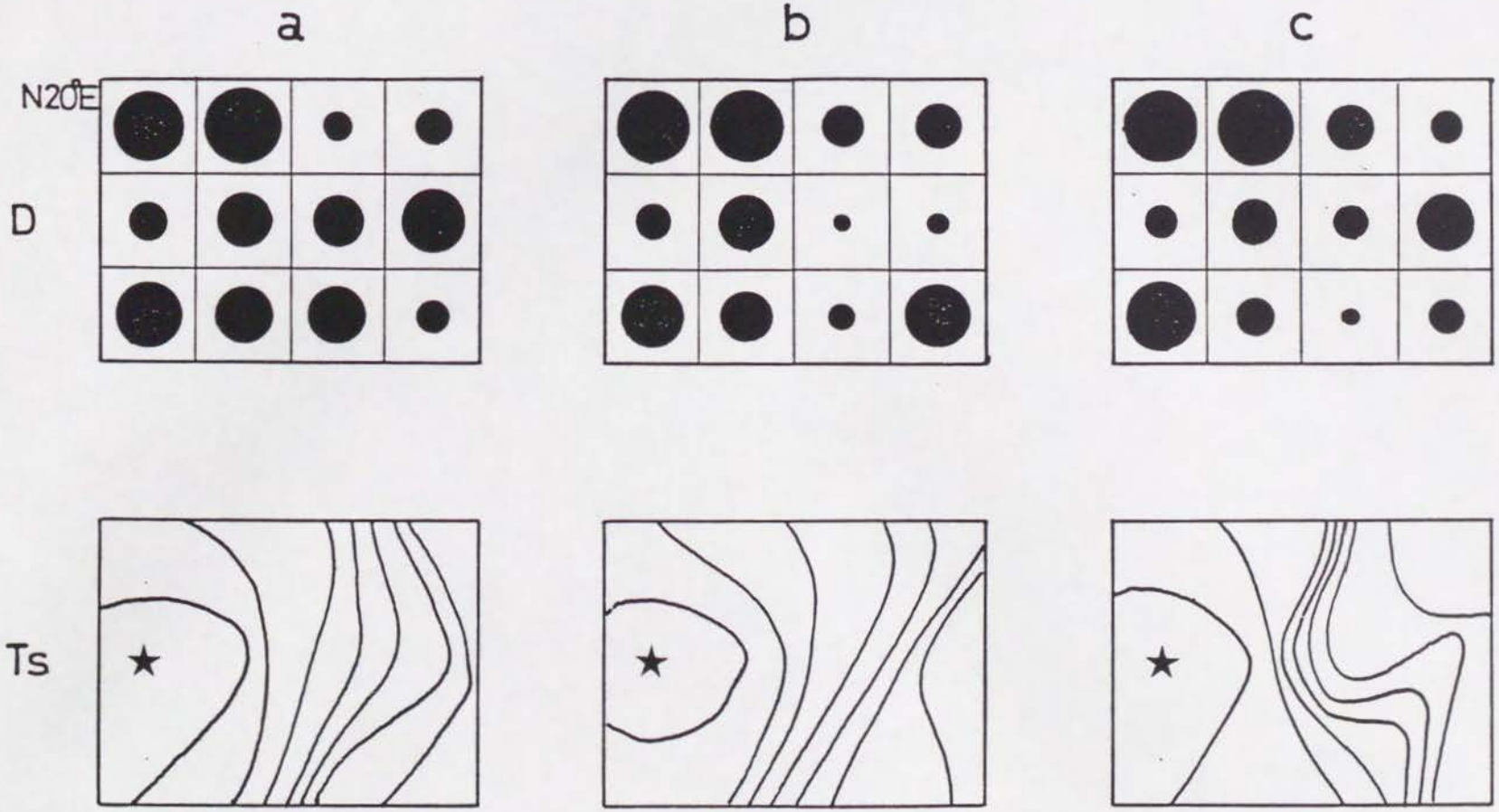

Fig. 18

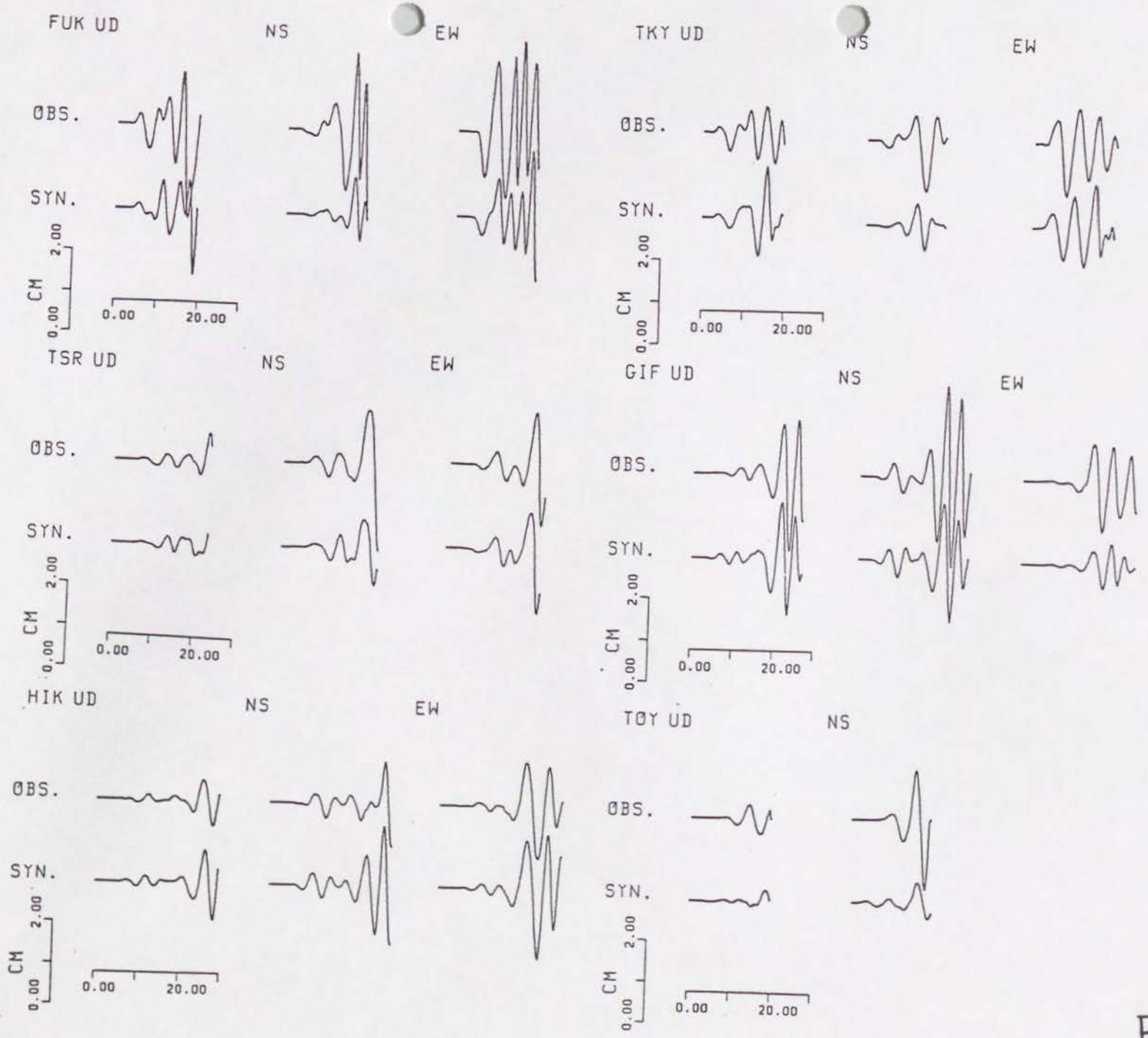
FUK UD
NS
EW
OBS.
SYN.
CM
2.00
0.00
0.00
20.00
TKY UD
NS
EW
OBS.
SYN.
CM
2.00
0.00
0.00
20.00
TSR UD
NS
EW
OBS.
SYN.
CM
2.00
0.00
0.00
20.00
GIF UD
NS
EW
OBS.
SYN.
CM
2.00
0.00
0.00
20.00
HIK UD
NS
EW
OBS.
SYN.
CM
2.00
0.00
0.00
20.00
TOY UD
NS
OBS.
SYN.
CM
2.00
0.00
0.00
20.00

Fig. 19

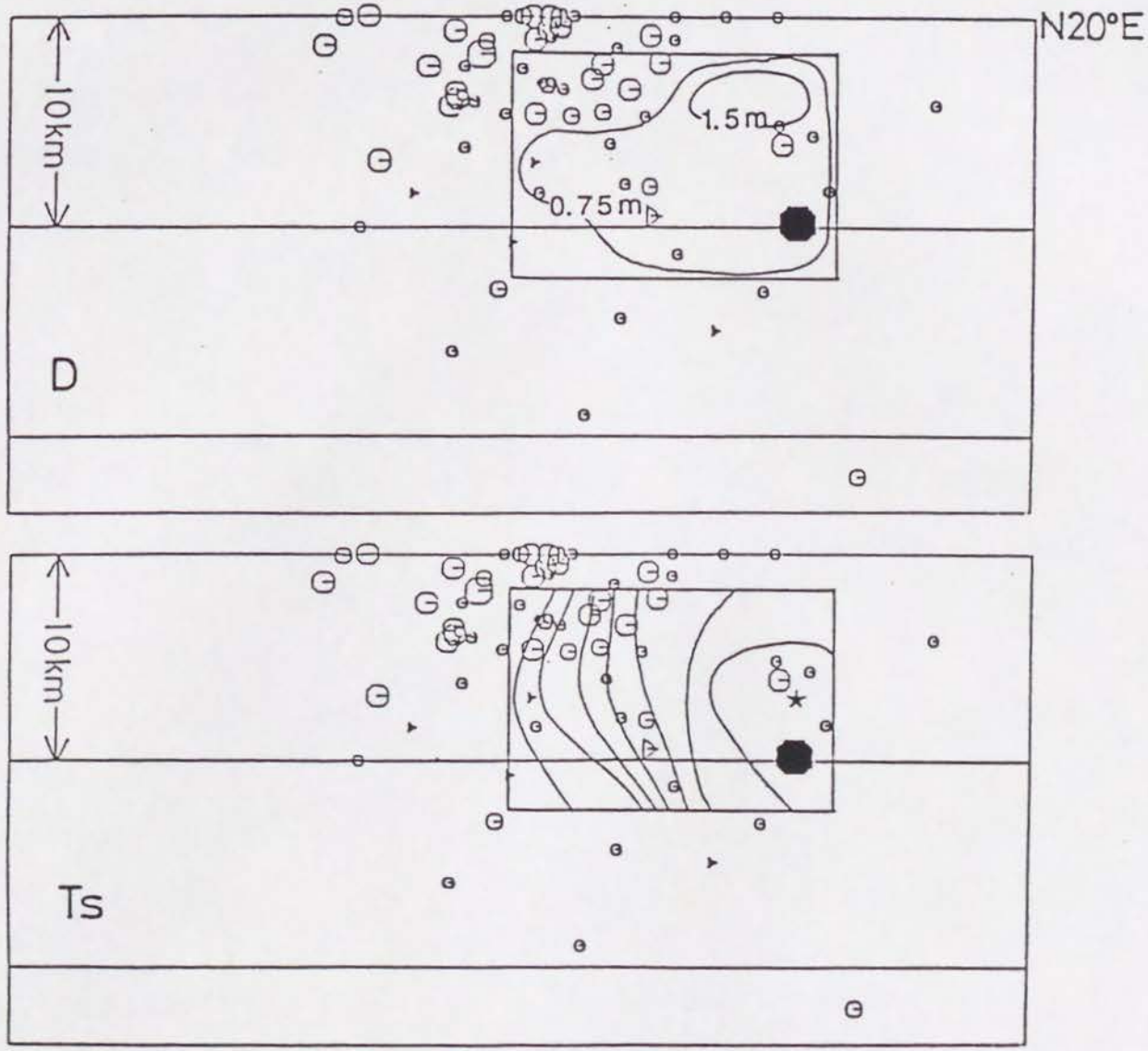

Fig. 20

The 1984 NaganoKen-Seibu earthquake

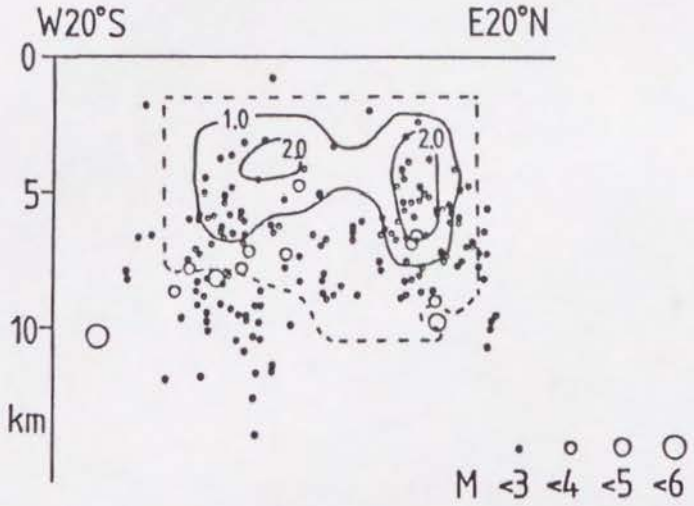

The 1969 GifuKen-Chubu earthquake

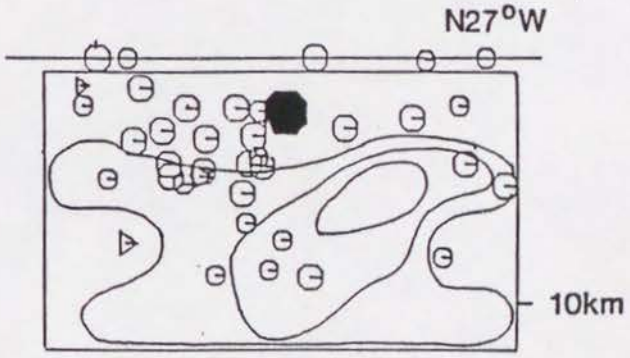

The 1961 Kita-Mino earthquake

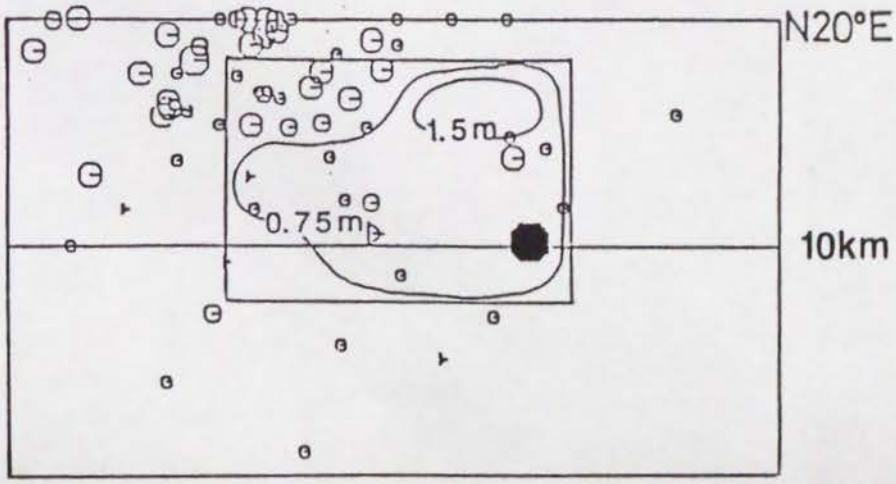

Fig. 21

The 1984 NaganoKen-Seibu earthquake

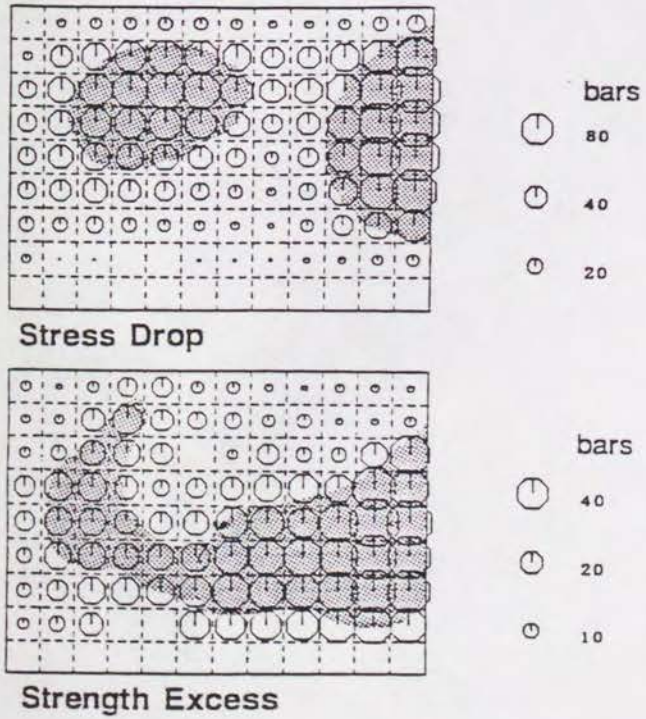

The 1969 GifuKen-Chubu earthquake

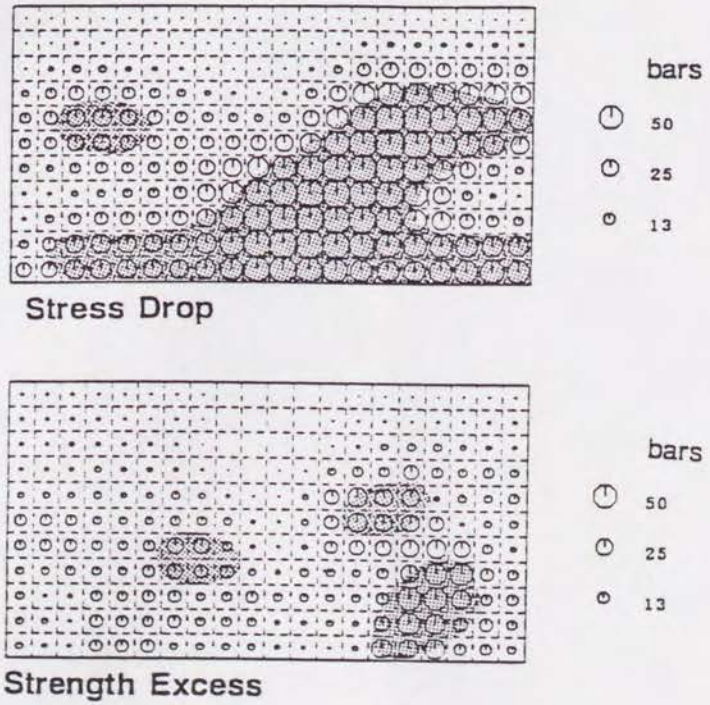

The 1961 Kita-Mino earthquake

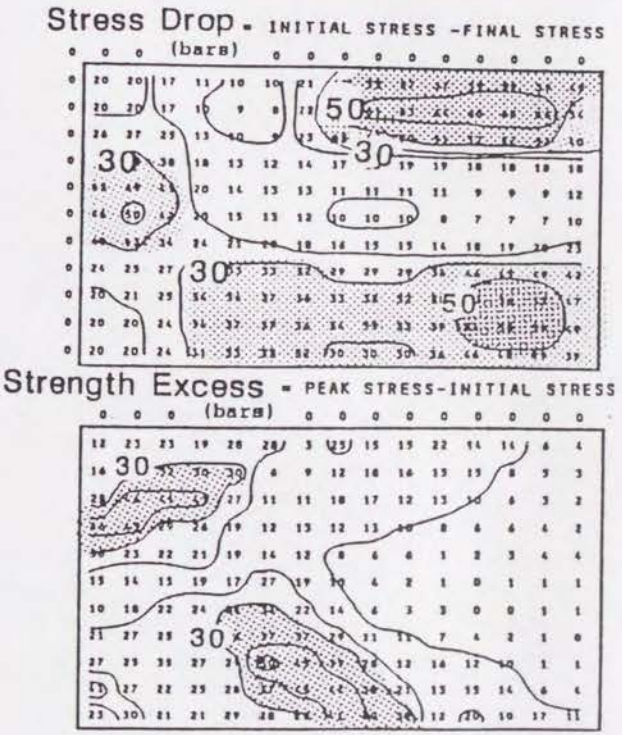

Fig. 22

Table 1 Kinematic fault parameters obtained for the three earthquakes.

Eerthquake	Moment ($\times 10^{25}$ dyne·cm)	l (km)	w (km)	D (m)	D_{max} (m)	T (s)	strike	dip	slip
NaganoKen-Seibu 1984 Sep. 14 M6.8	4.0	12	6	1.4	2.0	3	250°	72°	170°
GifuKen-Chubu 1969 Sep. 9 M6.6	5.4	20	11.2	0.7	1.7	6	153°	90°	0°
Kita-Mino 1961 Aug. 19 M7.0	5.0	16	12	0.9	1.6	8	290°	60°	130°

l ; fault length
w ; fault width
D ; average dislocation
D_{max} ; maximum dislocation
T ; source duration time